Cell

RAF-like protein kinases mediate a deeply conserved, rapid auxin response

Graphical abstract

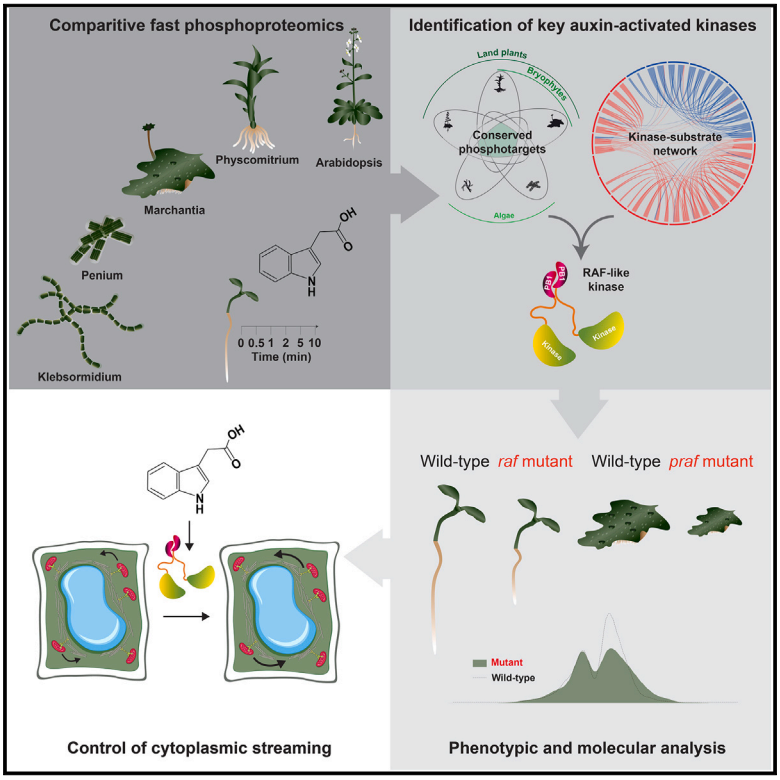

Highlights

- Auxin triggers rapid (<30 s) and specific proteome phosphorylation changes
- Fast auxin-triggered phosphorylation is ancient and widespread in the green lineage
- Phosphorylation-based auxin signaling is mediated by B4 RAF-like kinases
- RAF-like kinases connect fast auxin signaling to cytoplasmic streaming

Authors

Andre Kuhn, Mark Roosjen, Sumanth Mutte, ..., Joris Sprakel, Jiří Friml, Dolf Weijers

Correspondence

dolf.weijers@wur.nl

In brief

The molecule auxin triggers fast and specific protein phosphorylation changes in land plants and algae. This ancient and widespread response is mediated by conserved B4 RAF-like kinases that connect rapid signaling to cellular auxin responses such as the acceleration of cytoplasmic streaming.

Kuhn et al., 2024, Cell *187*, 130–148
January 4, 2024
https://doi.org/10.1016/j.cell.2023.11.021

CellPress

CellPress
OPEN ACCESS

Cell

Article

RAF-like protein kinases mediate a deeply conserved, rapid auxin response

Andre Kuhn,[1,7] Mark Roosjen,[1,7] Sumanth Mutte,[1] Shiv Mani Dubey,[2] Vanessa Polet Carrillo Carrasco,[1] Sjef Boeren,[1] Aline Monzer,[3] Jasper Koehorst,[4] Takayuki Kohchi,[5] Ryuichi Nishihama,[6] Matyáš Fendrych,[2] Joris Sprakel,[1] Jiří Friml,[3] and Dolf Weijers[1,8,*]

[1]Laboratory of Biochemistry, Wageningen University, Stippeneng 4, Wageningen, the Netherlands
[2]Department of Experimental Plant Biology, Charles University, Prague, Czech Republic
[3]Institute of Science and Technology Austria, Klosterneuburg, Austria
[4]Laboratory of Systems and Synthetic Biology, Wageningen University, Wageningen, the Netherlands
[5]Graduate School of Biostudies, Kyoto University, Kyoto, Japan
[6]Department of Applied Biological Science, Faculty of Science and Technology, Tokyo University of Science, Noda, Chiba, Japan
[7]These authors contributed equally
[8]Lead contact
*Correspondence: dolf.weijers@wur.nl
https://doi.org/10.1016/j.cell.2023.11.021

SUMMARY

The plant-signaling molecule auxin triggers fast and slow cellular responses across land plants and algae. The nuclear auxin pathway mediates gene expression and controls growth and development in land plants, but this pathway is absent from algal sister groups. Several components of rapid responses have been identified in Arabidopsis, but it is unknown if these are part of a conserved mechanism. We recently identified a fast, proteome-wide phosphorylation response to auxin. Here, we show that this response occurs across 5 land plant and algal species and converges on a core group of shared targets. We found conserved rapid physiological responses to auxin in the same species and identified rapidly accelerated fibrosarcoma (RAF)-like protein kinases as central mediators of auxin-triggered phosphorylation across species. Genetic analysis connects this kinase to both auxin-triggered protein phosphorylation and rapid cellular response, thus identifying an ancient mechanism for fast auxin responses in the green lineage.

INTRODUCTION

The plant-signaling molecule auxin is key to numerous growth and developmental processes in plants.[1] Iconic auxin-dependent processes are the tropic growth responses to light and gravity,[2–5] differentiation of vascular strands, and the control of fruit development.[6–9] The dominant naturally occurring auxin is indole 3-acetic acid (IAA), a chemically simple tryptophan derivative that land plants can synthesize, but is widely found across both prokaryotic and eukaryotic species.[10] Its biological activity in plants as a signaling molecule, acting at nanomolar to micromolar concentrations, is extremely profound. Auxin can trigger a wide range of physiological, cellular, and molecular changes that likely underlie the long-term effects on plant growth and development. Although initial discoveries with auxin were made in flowering plants, the occurrence of IAA and physiological and developmental responses to the molecule have been reported well beyond this group. All land plants studied,[11] and a range of algae,[12–15] show responses to externally applied auxin, which suggests a very deep origin of the capacity to respond to auxin. The cellular responses to auxin come in two flavors—fast and slow. The fast responses include changes in membrane polarization,[16–18] cytoplasmic streaming,[19,20] calcium and proton fluxes,[21–25] and trafficking.[26] Slower responses include cellular growth, division, and differentiation.[27–30]

Using the ability of auxin to inhibit root growth in the flowering plant *Arabidopsis thaliana*, a set of components was identified that mediates auxin's activity in regulating gene expression—the nuclear auxin pathway (NAP).[31–35] This system revolves around the auxin-triggered proteolysis of a family of transcriptional repressor proteins, thus liberating DNA-bound transcription factors and allowing gene regulation.[36] Through this pathway, auxin controls the expression of hundreds to thousands of genes, and mutations in its components interfere with most, if not all developmental auxin functions, culminating in embryo lethality in the most strongly affected mutants.[37–39]

From analysis of the evolutionary history of the auxin response systems, it appeared that the same auxin response system acts to control gene expression and development across land plants.[11,40] However, it is also clear that the closest sister group to land plants—the streptophyte algae—do not carry the NAP, in cases even lacking all its components.[11] Thus, a major unanswered question is how algae can respond to auxin in the absence of the known auxin response system. In addition, the fastest gene

expression responses to auxin have been recorded in 5–10 min,[41,42] but several of the fast responses[19,20,24,43,44] occur well within the time needed for gene expression and protein synthesis. Thus, it is likely that the currently known auxin response system represents the "slow" branch and that a separate, currently unknown system must exist to mediate fast responses. Analysis of fast responses, including plasma membrane depolarization, apoplastic pH changes, calcium influx, and root growth inhibition in a number of Arabidopsis mutants surprisingly showed that the NAP receptors TIR1 and AFB1 mediate several fast responses.[18,43–46] This may in part be related to the recently reported adenylate cyclase activity in TIR1.[47] The existence of fast auxin responses in land plants and their algal sisters would predict a fast response system to be shared between these clades. TIR1 only evolved in land plants, and AFB1 evolved much later[11]; therefore, there must be other, potentially deeply conserved mechanisms for fast response.

Protein phosphorylation is a widespread mechanism for enzymatically modifying the structure and function of pre-existing proteins,[48] thus eliminating the need for *de novo* protein synthesis. Given that phosphorylation depends only on the (allosteric) activation of a protein kinase, the reaction is intrinsically rapid. Several well-known examples of phosphorylation-based signaling exist across the kingdoms of life.[49–52] Among these, some are particularly rapid, with insulin and epidermal growth factor (EGF) ligands triggering initial phosphorylation changes by receptor kinases within seconds,[51,52] followed by relays and amplification steps with additional protein kinases.[52] Phosphorylation-based signaling is also widespread in plants and mediates responses to peptide ligands in development and immunity,[50] as well as to brassinosteroids.[53–55] Recently, we found that in Arabidopsis roots, IAA can trigger changes in phosphorylation of many proteins within 2 min,[19,24] which opens the possibility that a phosphorylation-based mechanism underlies rapid auxin responses. This phosphorylation response requires the AUXIN BINDING PROTEIN1 (ABP1)[19] and TRANSMEMBRANE KINASE1 (TMK1) proteins, of which at least ABP1 is conserved across land plants and algae.[56] It is therefore possible that phosphorylation-based signaling not only represents a mechanism for fast response but also represents the predicted deeply conserved auxin response system.

Here, we asked if this auxin response may represent the elusive, deeply conserved mechanism underlying rapid cellular responses. We find that auxin triggers rapid changes in protein phosphorylation in 5 different land plant and algal species, including a core set of conserved targets. We leveraged both dense temporal and comparative datasets to identify rapidly accelerated fibrosarcoma (RAF)-like kinases that mediate auxin-triggered protein phosphorylation and control of a fast cellular response across species. This work thus identifies an ancient system for rapid responses to the auxin signaling molecule that has a profound impact on many cellular pathways and functions.

RESULTS

Identification of deeply conserved cellular responses to auxin

Rapid cellular and physiological auxin responses have predominantly been studied in *Arabidopsis thaliana* (henceforth "Arabidopsis"), and it is unclear if any represent a conserved response. Among the fast auxin responses that have previously been recorded, two stand out as being potential candidates for being shared outside of land plants, and we first explored their conservation.

Membrane potential reflects the difference between cytoplasmic and apoplastic electrical potentials (Figure 1A). Auxin has a profound effect on membrane potential by triggering depolarization of plasma membrane,[18,25] followed by a hyperpolarization of the membrane.[18,24,57,58] Both membrane depolarization and hyperpolarization depend on auxin's ability to regulate ion fluxes across the plasma membrane, predominantly involving H^{+}-ATPase proton pumps and the cytoplasmic AFB1 receptor.[18,46] To first test whether this response is conserved in the plant lineage, we monitored membrane potential after 5 min of treatment with 100 nM IAA in Arabidopsis roots, *Marchantia polymorpha* (liverwort; henceforth "Marchantia") rhizoid initials in gemmae, and *Klebsormidium nitens* (algae; henceforth "Klebsormidium") filaments using the membrane potential fluorescent probe DISBAC2(3) that has been validated as a tool for reporting changes in membrane potential.[18,59] An increase in apoplastic DISBAC2(3) fluorescence reports membrane depolarization. We observed a significant increase in fluorescence upon auxin treatment in all three species (Figures 1B and 1C). Moreover, the relative increase was quantitatively very similar between species. This indicates that rapid auxin-triggered plasma membrane depolarization is a deeply conserved rapid auxin response.

Cytoplasmic streaming describes the actin cytoskeleton-mediated movement of organelles through the cytoplasm and is thought to have an essential function in the transport of nutrients and proteins within the cell.[60] In plants, cytoplasmic streaming is primarily driven by plant-specific myosin XI cytoskeletal motor proteins (Figure 1D). We examined the effect of treatment with 100 nM IAA on cytoplasmic streaming by monitoring the movement of fluorescently labeled mitochondria in epidermal cells of Arabidopsis roots within the elongation zone, as well as in Marchantia rhizoid cells (Figure 1E). After particle tracking, we determined the active diffusion rate (K) and diffusive exponent (α) of mobility by fitting mean square displacements, ensemble-averaged per cell, to an anomalous diffusion model.[61,62] We found consistent streaming in both species (Figure 1F; Videos S1 and S2), but absolute rates differed between species (Figures 1F, S1A, and S1B). Pretreatment with the actin-depolymerizing drug Latrunculin B reduced cytoplasmic streaming in both species (Figures S1C and S1D), confirming that the motion observed is actin-dependent. Importantly, auxin treatment consistently increased the diffusion rate in both species (Figure 1F; Videos S1 and S2). Hence, like membrane depolarization, the acceleration of cytoplasmic streaming is a deeply conserved response to auxin.

Identification of a deeply conserved, rapid, phosphorylation-based auxin response

The finding that membrane depolarization and cytoplasmic streaming are similarly influenced by auxin across land plants and algae suggests the existence of a shared mechanism for auxin perception and signal transduction. We therefore explored

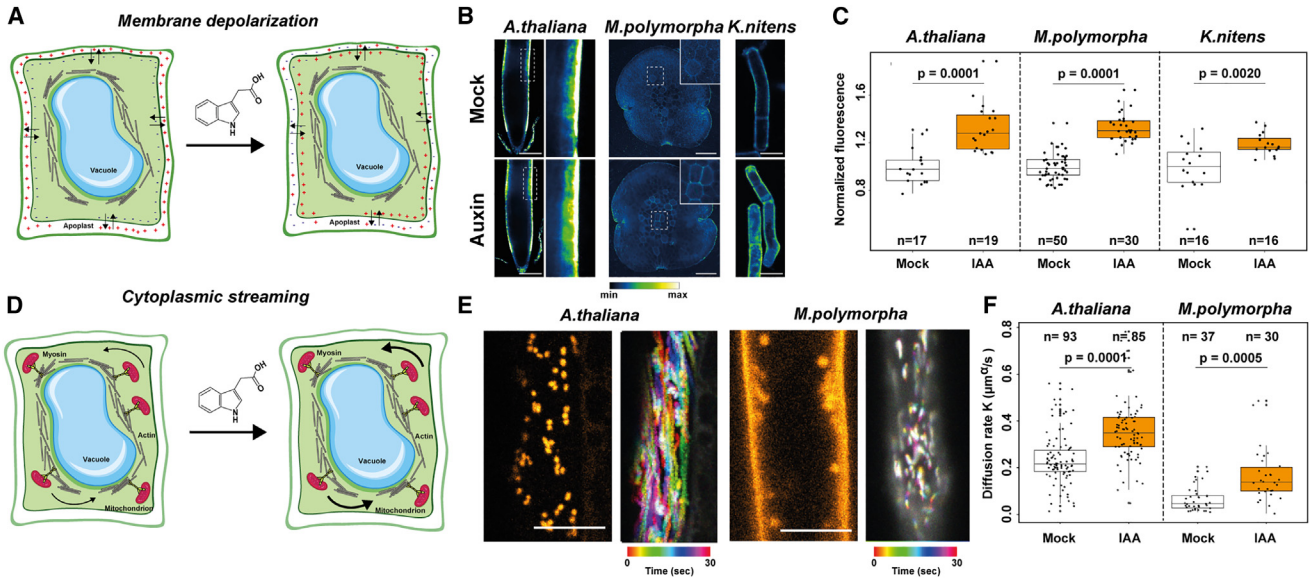

Figure 1. Auxin triggers fast cellular and physiological responses across the plant kingdom

(A) Scheme depicting membrane depolarization.

(B) Representative images of membrane depolarization measured using DISBAC2(3) fluorescence in control (mock) and IAA-treated Arabidopsis root cells (scale bars, 100 μm), Marchantia rhizoid initial cells (scale bars, 100 μm), and Klebsormidium cells (scale bars, 10 μm).

(C) Quantification of normalized fluorescence intensities across replicates.

(D) Scheme depicting cytoplasmic streaming.

(E) Representative images of Arabidopsis root epidermis cells and Marchantia rhizoid cells stained with the mitochondria stain rhodamine 123 (scale bars, 10 μm). Each left image shows a single frame, and the right image shows an overlay of a color-coded set of frames over time.

(F) Diffusion rate K ($\mu m^{\alpha}/s$) in control (mock) and IAA-treated Arabidopsis root cells and Marchantia rhizoid cells. Boxplots are shown along individual measurements, number of observations (n) is indicated, and significance (Student's t test) is shown. See also Figure S1 and Videos S1 and S2.

whether rapid phosphorylation response is conserved beyond Arabidopsis. We selected a set of phylogenetically distant species ranging from bryophytes to green algae for phosphoproteomic analysis. These included the bryophytes Marchantia and *Physcomitrium patens* (moss; henceforth "Physcomitrium") and the streptophyte algae Klebsormidium and *Penium margaritaceum* (henceforth "Penium"), in addition to the angiosperm Arabidopsis. This selection encompasses both early-diverging streptophyte algae (Klebsormidium) and a close sister to land plants (Penium; Zygnematophyceae) and covers two clades within the bryophytes: liverworts (Marchantia) and mosses (Physcomitrium). Notably, sporophytic (root) tissue was sampled for Arabidopsis, while gametophytic tissue was sampled for all other species. Consequently, the suite of species not only spans phylogeny but also haploid and diploid generations and a wide array of different cell and tissue types. All species were treated with the same concentration (100 nM) of IAA, followed by phosphopeptide enrichment after 2 min and mass spectrometry. Strikingly, we find that 2 min of auxin treatment leads to large shifts in the phospho-proteome in all species tested (Figure 2A). The number of differential phosphosites was comparable across species (at false discovery rate [FDR] $\geq$ 0.05: n = 1,048 in Arabidopsis; n = 670 in Physcomitrium; n = 741 in Marchantia; n = 719 in Penium; and n = 1,231 in Klebsormidium). In all species except Klebsormidium, hyperphosphorylation upon auxin treatment represented the majority of differential phosphosites (64% in Arabidopsis, 76% in Physcomitrium, 73% in Marchantia, and 60% in Penium), whereas hyper- and hypo-phosphorylation were more equal in Klebsormidium (47% hyperphosphorylation) (Figure 2A). Thus, rapid, global changes in phosphoproteomes are triggered by auxin at comparable scales in all species tested.

We next asked if the cellular functions and proteins that are targeted by auxin-triggered phosphorylation changes are conserved among the species tested. Estimated divergence times of the species used here from common ancestors are around 850 Mya for algae and land plants and 500 Mya among the land plants.[63] Given these enormous evolutionary distances, there is substantial sequence divergence within protein families and large differences in gene family sizes.[64] This makes establishing direct orthology relationships very challenging. Therefore, before comparing differential phosphoproteins at the protein/family level, we constructed a set of orthogroups that represent the set of genes that originated from a single gene in the last common ancestor of all the species under consideration. We then consider members of the same orthogroup to represent a conserved ancestral function. Among the species tested, Penium has a remarkably large number of orthogroups with multiple members (Figure S2A), which likely reflects the high degree of fragmentation of the genome assembly.[65] In all species, about half of the phosphoproteins are unique to that species, and the other half is shared with one or more other species (Figure 2B). We identified sets of proteins that are commonly regulated among land plants (n = 193), bryophytes (n = 304), or algae (n = 262). In addition, we found an overlap of 11 orthogroups

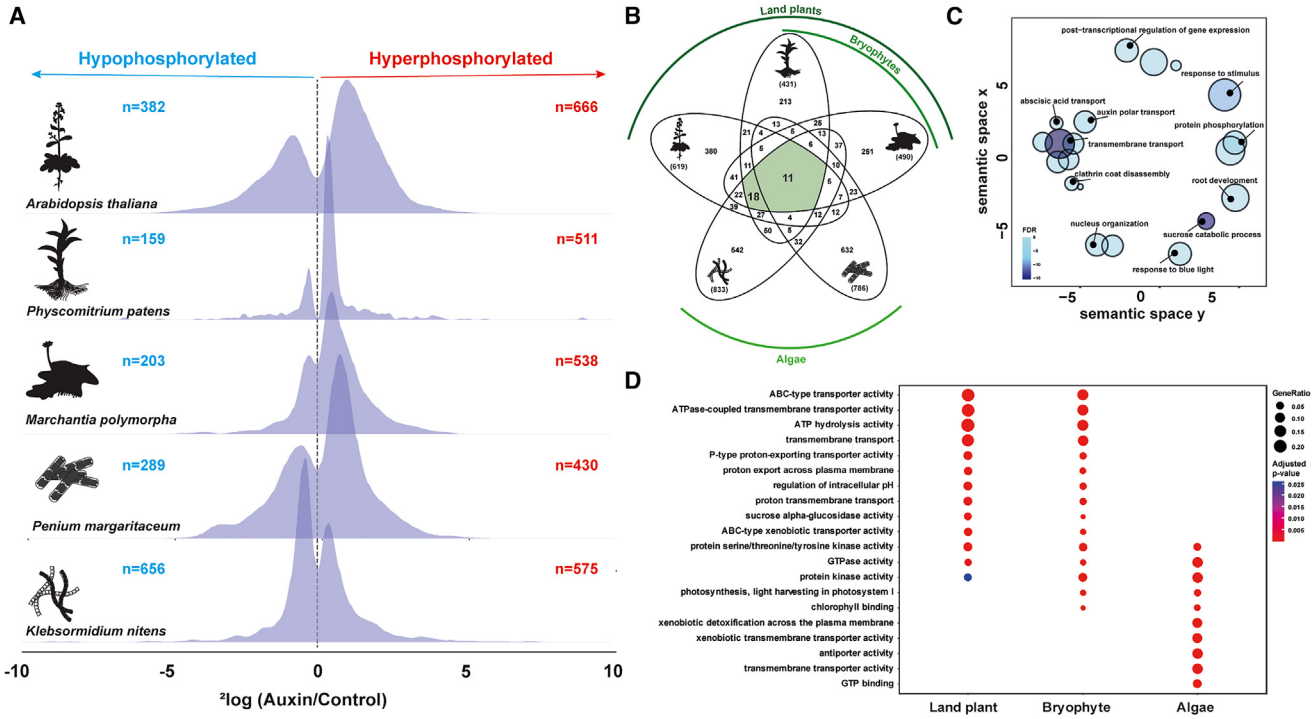

Figure 2. Comparative phosphoproteomics identifies a rapid and conserved auxin response

(A) Distribution histograms of significantly differential phosphosites (FDR $\leq$ 0.05) comparing 2 min of 100 nM IAA treatment with mock treatment across 5 species. Numbers of hyper- or hypo-phosphorylated sites are indicated.

(B) Venn diagram with numbers of orthogroups found as differentially phosphorylated upon IAA treatment across species.

(C) Reduced GO analysis of the 29 shared orthogroups (green in B). Circle sizes correspond to gene count within orthogroups.

(D) GO-term enrichment of terms within land plants, bryophytes, and algae. See also Figure S2.

across all organisms (Figures 2B and S2B). Given the fragmentation of the Penium genome assembly, we also consider orthogroups shared by all species except Penium to represent potential universally shared targets. When excluding Penium from the analysis, we found 29 orthogroups to be shared (Figure 2B). Note that, given the large evolutionary distance and varying degrees of primary sequence conservation, we focused on shared phosphoproteins rather than phosphosites. We next explored functional annotations of shared phosphoproteins for each intersection through gene ontology (GO) analysis. There was a large difference between the functions enriched in land plants and algae (Figures 2D and S2C). Comparing land plants with only bryophytes showed that some functions are unique to bryophytes (“photosynthesis” and “chlorophyll binding”) and that most are shared. Algae not only share a set of functional enrichment with land plant plants (or only with bryophytes) but also show a range of algae-specific functions, notably including membrane transporters. Collectively, a large set of processes seems to be targeted by auxin-regulated phosphorylation.

We next focused our attention on the core set of deeply conserved phospho-targets. Analysis of these orthogroups showed that a broad range of cellular functions is subject to auxin regulation (Figure 2C). These include processes at the plasma membrane or endomembranes, such as transmembrane transport and clathrin coat disassembly, and also nuclear organization and posttranslational regulation of gene expression. Furthermore, GO analysis identified responses to external stimuli and hormones, including responses to blue light, abscisic acid transport, and polar auxin transport. As expected from a phospho-proteomic analysis, protein phosphorylation was another highly enriched GO term. Thus, comparative phosphoproteomics shows that auxin triggers species-specific and deeply conserved phosphorylation responses.

Auxin phospho-response is rapid and dynamic

The vast effect of a 2-min treatment with a low IAA concentration on the phosphoproteome in phylogenetically distant species is striking and suggests this to be a specific signaling response. However, auxin is a weak organic acid derived from tryptophan, and it is possible that (part of) the response observed is an unspecific response to weak organic acids or auxin-like molecules. To test chemical specificity, we therefore used a panel of related chemicals (all at 100 nM) and measured phosphoproteomes after 2 min of treatment in Arabidopsis roots. None of the synthetic auxin analogs 2,4-dichlorophenoxy-acetic acid (2,4D), 1-naphtaleneacetic acid (1-NAA), or 2-naphtaleneacetic acid (2-NAA) triggered phosphorylation changes that showed any correlation to those induced by IAA (Figure S3A). Likewise, neither benzoic acid (BA) nor formic acid (FA) induced IAA-like phosphorylation changes (Figure S3A). As a control, two entirely independent IAA treatments and measurements (Figure S3B) showed a strong correlation. Thus, IAA phospho-response seems

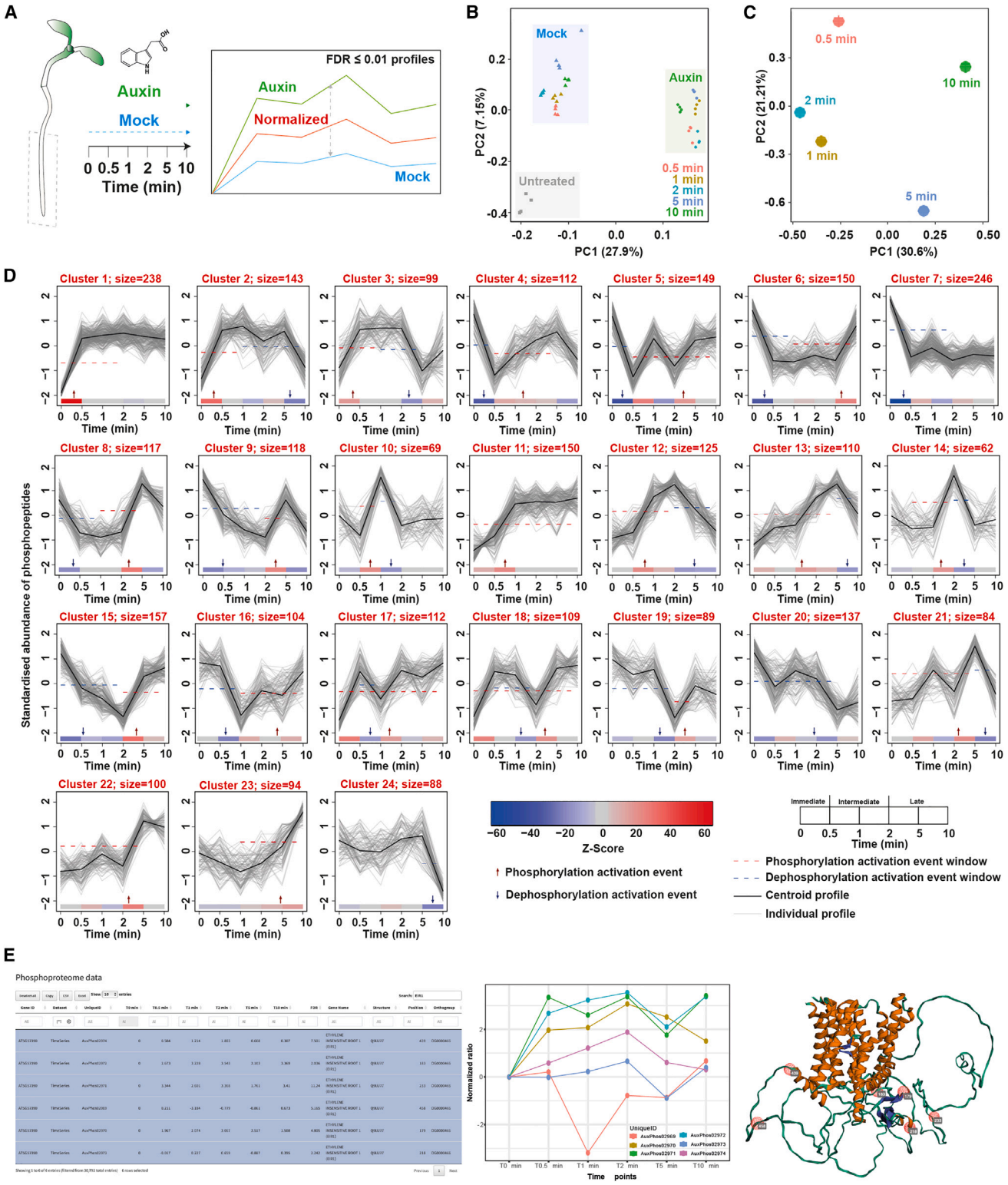

Figure 3. Dynamics of auxin phosphoresponse in Arabidopsis

(A) Schematic overview of treatment, time, and analysis procedure.

(B and C) Principal-component analysis of all (untreated, mock, and auxin) replicates for all time points and (C) principal-component analysis of normalized IAA-responsive profiles.

(legend continued on next page)

chemically specific. Synthetic auxins have auxinic activity in several physiological assays, and it is therefore striking that 2,4-D, 1-NAA, and 2-NAA failed to trigger IAA-like phosphorylation changes. To test if these can act like IAA in this response, albeit less efficiently, we measured phosphoproteomes at a 10-fold higher concentration (1 μM). Indeed, at this concentration, 1-NAA and 2-NAA could induce IAA-like phosphorylation changes, but BA could not (Figure S3C). Finally, we confirmed that the changes in phosphopeptide abundance were not correlated to changes in overall protein abundance (Figure S3D). Thus, IAA induces a rapid phosphorylation response in Arabidopsis roots that shows chemical specificity to active auxins and is most effectively induced by the naturally occurring IAA.

The differential effects that IAA, synthetic auxins, and BA have on the phosphoproteome allow testing whether this response is related to the rapid cellular responses. Given that it has been shown that besides BA, 1-NAA and 2-NAA fail to trigger membrane depolarization,[18,44] it is likely that this response is not directly connected to auxin-triggered phosphorylation. We therefore compared the effect of 1-NAA, 2-NAA, and BA with that of IAA on cytoplasmic streaming. We found a striking similarity in the effect that these compounds had on cytoplasmic streaming and the phosphoproteome. At 100 nM, only IAA accelerated streaming, whereas none of the other compounds had a significant effect (Figure S3E). At 1 μM, however, 1-NAA and 2-NAA accelerated streaming, similar to IAA, whereas BA did not have any effect. Therefore, the chemical specificity and effectivity of these compounds on phosphoproteomics and cytoplasmic streaming suggest a strong relation between the two responses.

To explore the temporal dynamics of the phosphorylation response, we generated a time series of IAA treatments on Arabidopsis roots, ranging from 30 s to 10 min. To ensure that this time series was not confounded by auxin-independent effects of submerging roots in the growth medium, we also sampled solvent mock controls for each time point and subtracted the change in phosphosite abundance in the mock treatment from each IAA treatment (Figure 3A). This led to a set of phosphoproteomes that could be clearly resolved by principal-component analysis (PCA; Figure 3B). PCA analysis underlined the need for the use of mock solvent controls and showed a high degree of reproducibility across replicates. Strikingly, even at 30 s, IAA triggered changes in the abundance of hundreds of phosphosites (Figure 3C), underlining the rapid nature of the response. Compiling all differentially phosphorylated sites across the entire time series, a total of 2,962 phosphosites are regulated by IAA (Figure 3D), corresponding to 1,770 proteins, representing ~5% of the proteins encoded by the Arabidopsis genome.

We next used the Minardo-Model[66] to order groups of phosphopeptides that show similar trends of phosphorylation (Figure 3D). In each cluster, generalized linear models are derived from individual profiles, which, together with *Z* scores and post hoc Tukey tests, infer event windows at which the majority of profiles show half-maximal amplitude response. From this analysis, the earliest events likely occur well within 30 s after treatment (Figure 3D; clusters 1–9). This analysis clearly identified a range of temporal patterns in IAA-dependent phosphorylation (Figure 3D). These ranged from early (e.g., clusters 1–9), transient (e.g., clusters 10, 14, and 15), or late (e.g., clusters 23 and 24) hyper- or hypo-phosphorylation to gradual hyper- or hypo-phosphorylation (e.g., clusters 11–13) and oscillatory hyper- and hypo-phosphorylation (e.g., clusters 5, 17, 21, and 22). GO analysis on the clusters showed enrichment of different functions in the different phases of the response (Figure S3G).

The phosphorylation changes reported here offer a rich source of data that allows the development of hypotheses for future studies. To facilitate the use of this rich dataset and help interact with the data, we designed a webtool (AuxPhos; https://weijerslab.shinyapps.io/AuxPhos). AuxPhos allows searching individual proteins by their unique identifier and visualizing the quantification of their phosphopeptides across the various datasets. In addition to offering a searchable interface for navigating phosphoproteins, we have implemented AlphaFold2-based protein structural models to visualize phosphosites on predicted protein structures (e.g., Figure 3E). As further phosphoproteomic data will become available, these can be integrated into the tool.

Identification of kinases in auxin-triggered phosphoresponse

Given the availability of a densely sampled time series and the identification of nearly 3,000 phosphosites, we asked if the dataset could be used to infer phosphorylation relationships. Moreover, in combination with the auxin-dependent phosphoproteomes in a suite of evolutionarily distant species, it has the potential to identify conserved components that mediate rapid auxin responses.

We filtered the entire Arabidopsis phosphoproteome dataset for phosphosites in the (predicted[67]) kinase activation loops (Figure 4A). This identified 26 kinases that were differentially phosphorylated in their activation loop during the time series (Figure 4B), most of which were hyperphosphorylated and therefore likely activated. We next performed a regression analysis (Figure 4A) where we identified phosphorylation sites that temporally matched or followed the dynamics of activation of each kinase. This led to the generation of an inferred kinase-target network encompassing 23 kinases and 2,140 predicted phospho-targets (Figure S4A). To test the validity of this inference approach, we asked if protein kinases with known phospho-targets were correctly predicted. This analysis is challenging because of the relatively small number of well-documented kinase-substrate relationships with information about the exact phosphosite. Nonetheless, we found several such pairs to conform to their predicted relationship in our dataset

(D) Time series ordering of all FDR ≥ 0.01 $\log_2$ *Z* scored normalized auxin-responsive profiles. Clusters are ordered based on the earliest phosphorylation event. Phosphorylation event is based on the median time at which all individual profiles in a cluster cross half-maximal abundance within each event window (identified by the red or blue dashed line in graph and red and blue arrows on x axis, respectively).
(E) Screenshots of the R shiny app Auxphos. Selected profiles of a single protein can be selected and visualized in a plot, and phosphosites are mapped on a 3D predicted protein structure using AlphaFold2. See also Figure S3.

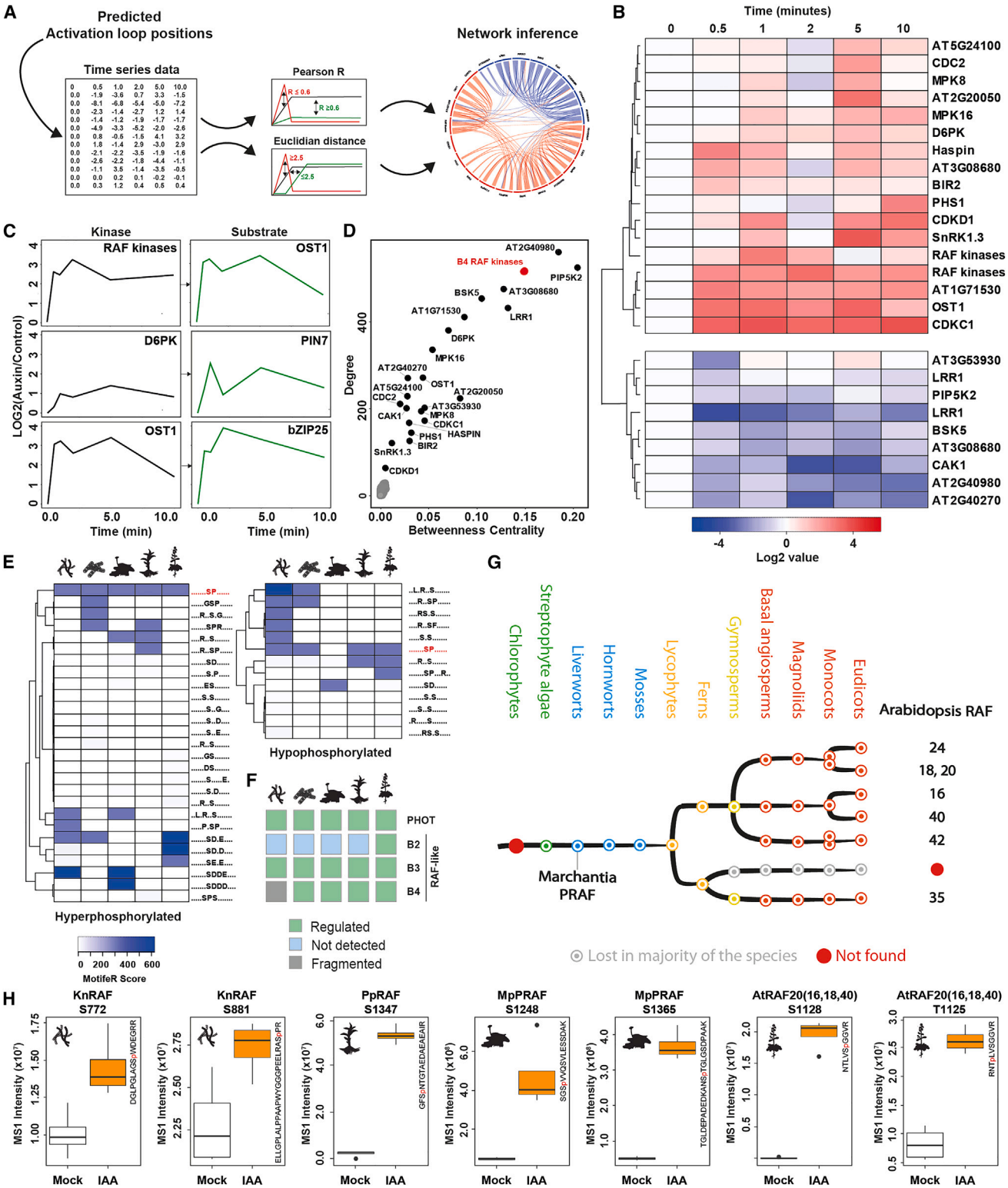

Figure 4. Identification of RAF-like kinases in rapid auxin response

(A) Schematic overview of the kinase network inference approach.

(B) Heatmap depicting the normalized intensity profiles of phosphopeptides in the activation loop of kinases.

(legend continued on next page)

(Figure 4C): an RAF-like kinase was connected to its OST1 target,[68] and this OST1 kinase to a bZIP target.[69] In addition, D6PK was connected to PIN7, consistent with PIN phosphorylation by this kinase.[70]

We next ranked the 23 kinases according to their weight and position in the phospho-network (Figure 4D), indicated by their degree and their betweenness centrality, parameters that were correlated in this network (Figure 4D). This identified several kinases as potential hubs in this network. These include the D6PK kinase and the LRR-RLK protein LRR1, a group of closely related B4 RAF kinases, and phosphoinositide kinase PIP5K2. It is an open question if the PIP5K activity or the membrane changes it induces are correlated with downstream phosphorylation. In any event, this network analysis offers a prioritized set of auxin-regulated kinases that are strong candidates for mediating rapid responses.

In parallel, to identify kinases that act on the conserved phosphorylation response across species, we compared the phosphosites among phospho-targets conserved in all species tested (Figure S4B). We observed only limited conservation of phospho-site level between conserved phospho-targets. This is not surprising, given the long evolutionary distance between the species tested. We therefore analyzed phosphorylation motifs enriched among the conserved phospho-targets. We found that hyperphosphorylation was associated with the presence of a proline-directed SP motif (Figure 4E), a motif typically targeted by mitogen-activated protein (MAP) kinases.[71,72] We next explored if any kinases are found among the conserved IAA-regulated phophotargets. We found three kinases in the core conserved set (Figure 4F): the blue light receptor PHOT1 (Figure 4F) and two RAF-like kinases, representing B3 and B4 subclades of the family.[73] Given that RAF-like kinases were also found as a hub in the network inference in Arabidopsis (Figure 4D), and given that these belong to the MAP kinase family that targets SP motifs, we consider these likely candidates for key components in the response.

RAF-like kinases are serine/threonine kinases that belong to the MAP kinase kinase kinase (MAPKKK) family.[73] Arabidopsis B2, B3, and B4 clade RAF-like kinases have been implicated in various physiological responses, including responses to hypoxia, osmotic stress, and drought.[68,74] The Marchantia B4 RAF-like kinase (PRAF) was implicated in the regulation of carbon fixation.[75] Although we found RAF-like kinases of the B2, B3, and B4 clade to be hyperphosphorylated after auxin treatment in Arabidopsis, it seems that only hyperphosphorylation in B3 and B4 clades is conserved (Figure 4F). Moreover, only the B4 RAF kinases were identified as a hub in the kinase network analysis (Figure 4D). Thus, given the multiple lines of evidence suggesting a role for B4 RAF-like kinases in auxin-triggered phosphorylation, we here focus on these.

We performed deep phylogenetic analysis and found that the B4 clade of RAF-like kinases is deeply conserved across streptophyte algae and land plants (Figure 4G). The family is represented by 7 paralogs in Arabidopsis, 2 in Physcomitrium, and single copies in Klebsormidium and Marchantia[76] (Figure 4G). Given the fragmented genome assembly in Penium, we could not unequivocally identify its ortholog. Importantly, most of the B4 RAF-like kinases are hyperphosphorylated in response to auxin treatment across species (Figure 4H), firmly connecting this family to auxin response.

B4 RAF-like kinases have conserved roles in growth, development, and auxin response

Given that no role for B4 RAF-like kinases in auxin response has been reported, we initially explored requirements for these proteins in auxin-associated growth and development, as well as in response to externally applied auxin. We analyzed previously established mutants: a septuple mutant of the entire Arabidopsis B4 clade (*raf*^{null}; also referred to as OK^{130} in Lin et al.[68]; here referred to as *raf*), and a null mutant in the single Marchantia ortholog (Mp*praf*^{KO} [75]; here referred to as *praf*). We found that in both species, loss of RAF activity caused growth and developmental phenotypes (Figures 5A–5L and S5A–S5F). In Arabidopsis, we found a range of defects in plant height (Figures 5A, 5B, and S5A), rosette area (Figures 5C, 5D, and S5B), root growth (Figures 5E, 5F, S5C, and S5D), and germination (Figures 5G, 5H, S5E, and S5F). In Marchantia, *praf* phenotypes manifested as smaller thallus size (Figures 5I, 5J, and S5G) and reduced gemmae cup number (Figures 5K and 5L), confirming earlier results.[75] All these phenotypes in both species were either fully or partially complemented by the introduction of individual *RAF20* or *RAF24* (Arabidopsis) or *PRAF* (Marchantia) copies, expressed from native genomic fragments and C-terminally fused to a fluorescent protein (Figures 5A–5L, S5A–S5D, and S5F). The fluorescent signals in these transgenic lines were broadly distributed to both membrane-associated and intracellular punctate structures (Figures 5M and 5N), perhaps related to the presence of a Phox-Bem1 (PB1) oligomerization domain in these proteins.[77]

Most growth phenotypes recorded in *raf* and *praf* mutants reflect processes that are known to involve auxin action.[30,78,79] We therefore tested sensitivity of the Arabidopsis *raf* and Marchantia *praf* mutants to auxin. In Arabidopsis, *raf* mutant roots were slightly less sensitive to growth inhibition by auxin (Figure 5O). Likewise, Marchantia *praf* mutant thallus, although already reduced in size under control conditions, was also less sensitive to auxin-induced growth inhibition (Figures 5P and S5H). Thus, in

(C) Plots showing normalized phosphopeptide abundance profiles along auxin time series of known kinase-substrate pairs recovered in the network inference approach.
(D) Network position of auxin-regulated kinases. Plot depicts degree (number of edges/interactions) and betweenness centrality.
(E) Clustering of phosphomotif enrichment scores of differential (FDR $\leq$ 0.05) phosphosites in all tested species.
(F) Heatmap depicting differential phosphosites (FDR $\leq$ 0.05) in PHOT and RAF-like kinases, in all species tested.
(G) Phylogeny of B4 RAF-like kinases. Arabidopsis numbering is indicated on the top. Every node represents an inferred ancestral gene copy at each divergence event.
(H) Raw MS1 intensities of B4 RAF-like kinase orthologues in mock- and IAA-treated samples. Phosphorylated residues and peptide sequence are indicated. See also Figure S4.

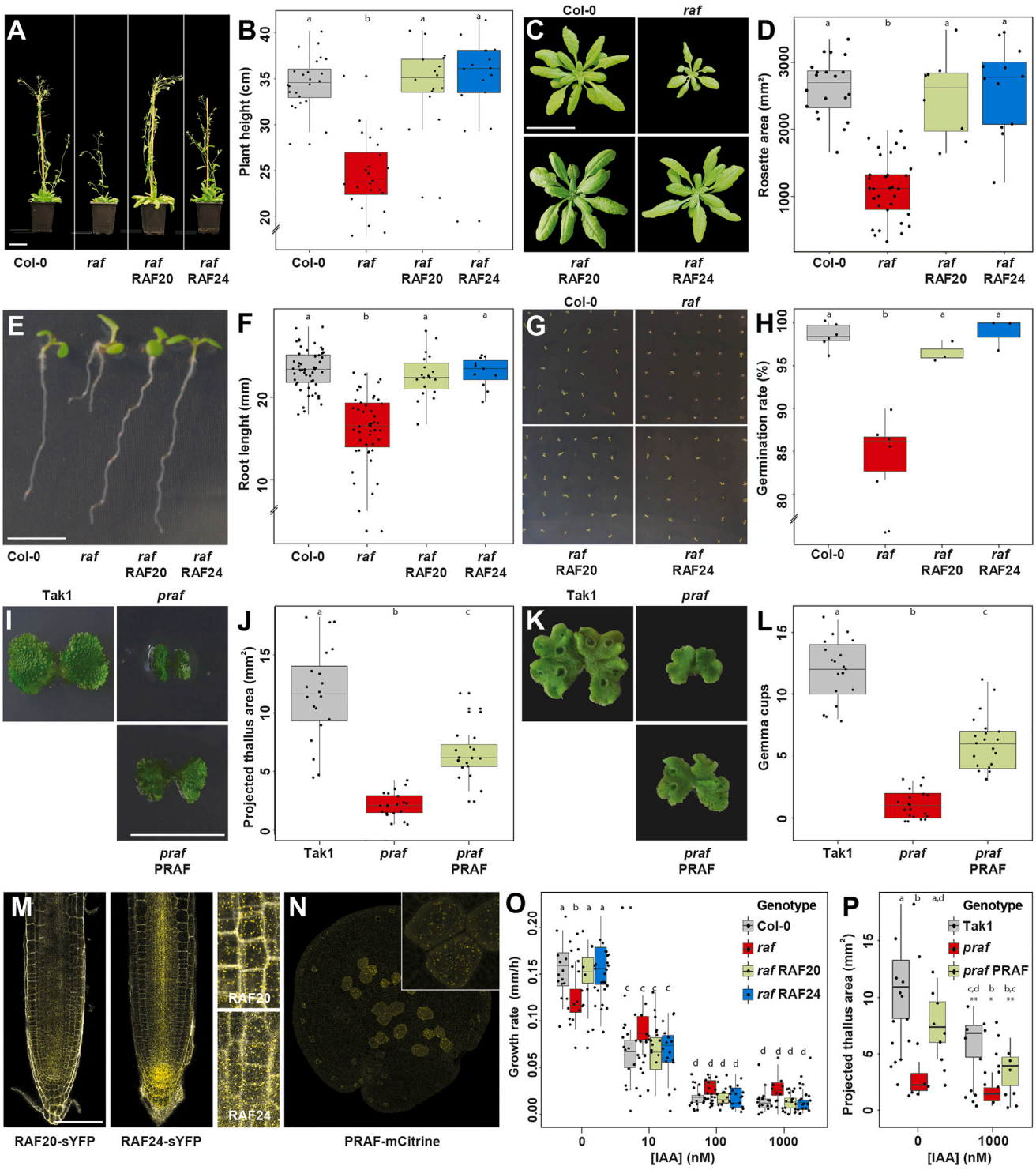

Figure 5. Phenotypes of *raf* mutants

(A–H) Characterization of phenotypes related to growth and development in Arabidopsis wild type (Col-0), *raf* mutant, and complemented *raf* mutant (with RAF20 of RAF24 transgene) and (I–L) in Marchantia wild type (Tak-1), *praf* mutant, and complemented *praf* mutant (with PRAF transgene). (A) Flowering plants and (B) quantification of shoot height. (C) Rosettes of 28-day-old plants and (D) quantification of rosette area. (E) 7-day-old seedlings and (F) quantification of root length. (G) Germinating seeds after 3 days and (H) quantification of germination rate. (I) Young thallus and (J) quantification of projected thallus area.
(K and L) (K) Older thallus and (L) quantification of gemmae cup number.
(M) Localization of pRAF20-RAF20-sYFP and pRAF24-RAF24-sYFP in Arabidopsis root tips (left: overview; right: magnifications).

(legend continued on next page)

both species, B4 RAF-like kinases act in growth and development and play a role in auxin response.

RAF-like kinases mediate fast auxin phospho-response

Auxin-associated growth and development are typically associated with changes in auxin-dependent gene expression through the NAP.[36,40] Given the auxin-related phenotypes in *raf* and *praf* mutants, we asked if these are affected in transcriptional responses. We therefore performed RNA sequencing (RNA-seq) in Arabidopsis (roots) and Marchantia (thallus) wild type (WT) and (*p*)*raf* mutants that were either treated with 1 μM IAA or with control medium for 1 h (Figures 6A–6D). This concentration of IAA should allow the detection of even subtle changes in transcription in mutants. In both species, transcriptomes under untreated conditions look very distinct between mutant and WT (Figures 6A and 6C), suggesting massive effects of loss of RAF function on the "baseline" transcriptome in the absence of externally applied auxin. However, comparing auxin-treated and untreated samples in both species showed substantial auxin-induced changes in transcriptomes in both WTs and mutants (Figures 6A and 6C). Indeed, analysis of individual auxin-regulated genes (Figures 6B and 6D) showed that mutants did not have an obvious defect in auxin-induced transcription. This suggests that RAF proteins do not have a major role in transcriptional auxin responses.

Given the rapid activation of RAF kinases by auxin (Figure 4B), it is conceivable that these kinases act in auxin response through their role in mediating rapid phosphorylation responses. We tested this hypothesis by subjecting *raf* mutants in Arabidopsis and *praf* mutant in Marchantia to phosphoproteomic profiling after 2 min of treatment with 100 nM IAA or control media. In both species, we found that the number of significant differentially hyperphosphorylated phosphosites after auxin treatment was reduced (666 in Arabidopsis WT; 445 in *raf* mutant; 538 in Marchantia WT; 285 in *praf*; Figure 6E). When comparing the identities of phosphosites in WTs and mutants, we found that 73% of the differential phosphosites in WT were lost in the Arabidopsis *raf* mutant, whereas 51% were lost in the Marchantia *praf* mutant (Figure 6E). We compared phosphoproteomes in non-treated mutants with WT controls in both species to identify functions that are deregulated in (*p*)*raf* mutants. In Arabidopsis *raf*, 392 orthogroups were different between mutant and WT, whereas in Marchantia *praf*, 785 orthogroups were differentially phosphorylated (Figure 6F). Many orthogroups that were not significantly affected by auxin in WT became differentially phosphorylated upon auxin treatment in the mutants (Figure 6G). This suggests that the mutants in both species not only lack a substantial part of auxin-triggered phosphorylation but also have a response system that is differently wired in non-treated conditions. It also shows that not all IAA-triggered phosphorylation changes are mediated by RAF-like kinases. These results are consistent with the large transcriptional changes in control-treated mutants and with the strong phenotypes in the mutants. When comparing targets of B4 RAF-dependent, auxin-triggered phosphorylation changes in the two species (453 and 240 orthogroups in Arabidopsis and Marchantia, respectively), we found a small overlap (24 orthogroups; Figures 6G and S6A). Given the evolutionary distance between Marchantia and Arabidopsis, this is remarkable since it suggests that there is indeed a set of conserved fast auxin responses under the control of a conserved mechanism. These shared, RAF/auxin-dependent targets included proteins associated with a diverse set of cellular processes (Figures 6H and S6B–S6D). This includes ion transport, membrane dynamics, and auxin export (e.g., PINs, ABCBs, and D6PK) but also features nuclear processes such as splicing and cytoplasmic processes such as cell plate formation and cytoskeleton organization (e.g., SPIKE1, TOR1, and NEK5). Finally, this analysis also identified previously reported phospho-targets of B4-type RAF kinases (e.g., VCS, VCR, and SE).[80]

To explore to what extent the auxin-triggered phosphorylation network is affected in (*p*)*raf* mutants, we compared the phosphorylation state of all kinases that were significantly hypo- or hyper-phosphorylated upon auxin treatment in WT of both species with their phosphorylation state in the mutants. Notably, most of the auxin-triggered kinase phosphorylation was lost (Figures 6I and 6J). This suggests that B4 RAF-like kinases directly or indirectly regulate the auxin-triggered phosphorylation of these kinases. Indeed, based on unique peptides, we found evidence for at least 5 of the 7 Arabidopsis B4 RAF-like kinases to be hyperphosphorylated in the auxin time series (Figure 6K), suggesting a profound role for the clade in the auxin-triggered protein phosphorylation network.

Proteins in the Arabidopsis RAF family have been identified as being hyperphosphorylated upon osmotic treatment[68] and to mediate response to hypoxia,[74] whereas Marchantia PRAF has a role in the response to altered photosynthesis.[75] We compared the 2-min auxin-triggered phosphorylation changes with the set of 973 phosphosites that are osmotic stress-responsive in Arabidopsis.[68] The overlap was very limited (37 phosphosites; Figure S6E), and 13 of these overlapping phosphosites depend on RAF (Figure S6E). We therefore conclude that the phospho-response that we identified here is specific and independent from osmotic stress responses and that RAF-like kinases mediate auxin-regulated phosphorylation response in both Arabidopsis and Marchantia.

(N) Localization of PRAF-PRAF-mCitrine in Marchantia gemma (inset: magnification).
(O) Root growth response to different concentrations of IAA in Arabidopsis wild type (Col-0), *raf* mutant, and complemented *raf* mutant (with RAF20 of RAF24 transgene).
(P) Projected thallus area of Marchantia type (Tak-1), *praf* mutant, and complemented *praf* mutant (with PRAF transgene) in the presence or absence of IAA. Dots in all graphs represent individual plants; scale bars are 5 cm (A) 5 cm (C), 10 mm (E), 10 mm (I), and 100 μm (M).
(A–L) Boxplots are shown along individual measurements, and significance (Student's t test) is shown, "a" indicates no significant difference to mutant, "b" indicates significant difference to wild type, and "c" indicates significant difference to both wild type and mutant ($p < 0.001$).
(O and P) Boxplots are shown along individual measurements, and significance (one-way ANOVA with Tukey HSD) is shown ($p < 0.05$).
(P) Significance (Student's t test) is shown to corresponding 0 nM IAA treatment (** $p < 0.01$, * $p < 0.05$). See also Figure S5.

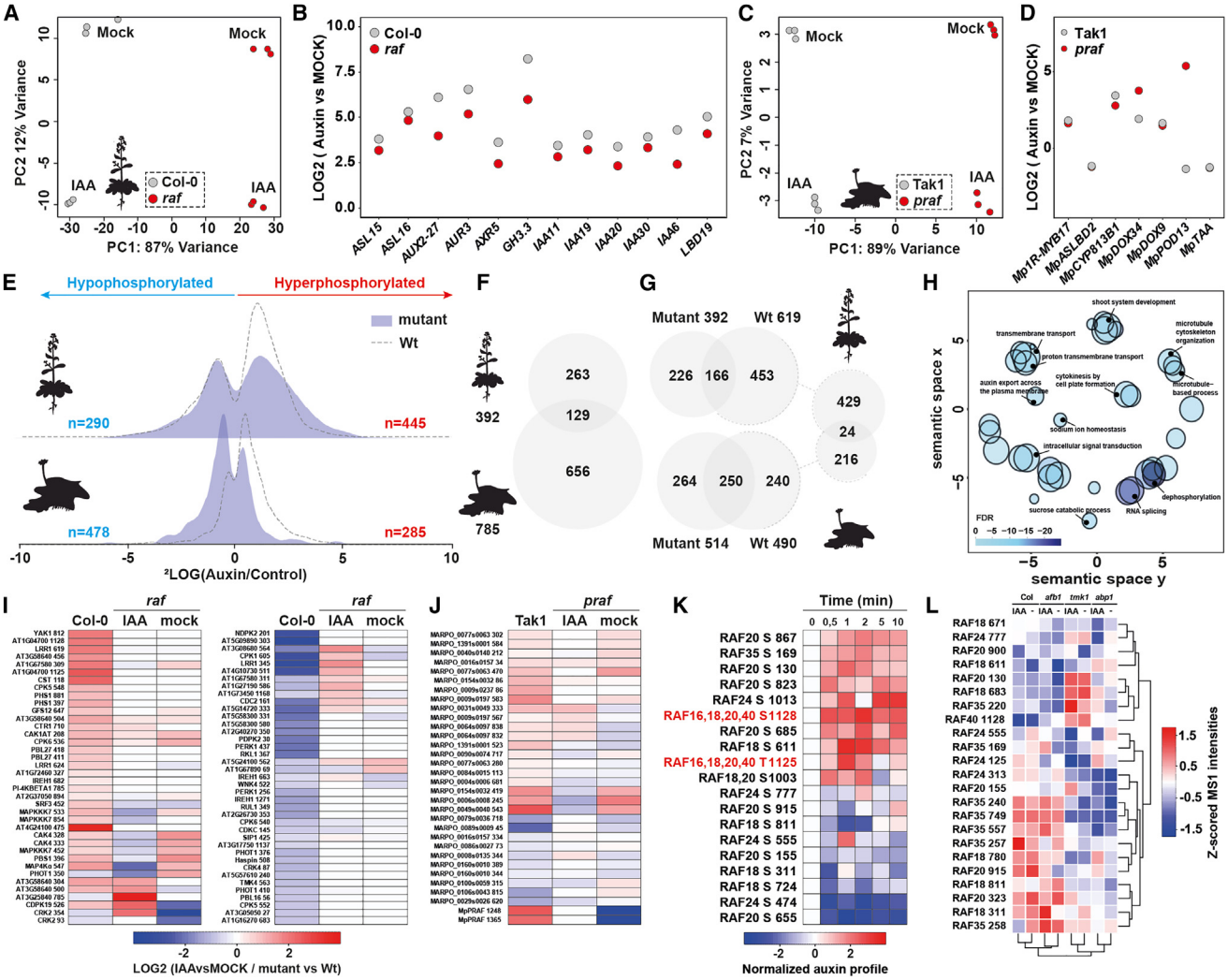

Figure 6. RAF-like kinases mediate auxin posphoresponse across land plant species

(A–D) RNA-seq analysis on wild type (Arabidopsis Col-0; Marchantia Tak-1) and *raf* (Arabidopsis, roots) and *praf* (Marchantia, gemmae) mutants treated with mock control or 1 μM IAA for 1 h. (A and C) PCA plots and (B and D) expression levels of individual, auxin-regulated genes.

(E) Distribution histograms of significant differential phosphosites (FDR ≤ 0.05) comparing 2 min of 100 nM IAA (auxin) treatment with mock treatment in wild type (dashed lines) and (*p*)*raf* mutant (solid area) in Arabidopsis roots (top) and Marchantia gemmae (bottom). Number of differential phosphosites is indicated.

(F) Venn diagrams indicating orthogroup overlap of differential phosphosites (FDR ≤ 0.05) in (*p*)*raf* mutants in Arabidopsis and Marchantia compared with respective wild types under mock condition.

(G) Venn diagrams indicating orthogroup overlap of differential phosphosites (FDR ≤ 0.05) in (*p*)*raf* mutants and wild types in Arabidopsis and Marchantia under IAA-treated conditions.

(H) Gene ontology analysis on the overlapping and conserved auxin- and (P)RAF-dependent proteins.

(I and J) Heatmap showing differential phosphorylation in Arabidopsis (I) and Marchantia (J) (*p*)*raf* null mutants of all kinases that are auxin-regulated in wild type.

(K) Heatmap showing phosphorylation profiles, normalized to the t = 0 time point, of Arabidopsis RAF kinases. Profiles marked in red are phosphosites located in the activation loop.

(L) *Z* scored MS1 intensities off all measured phosphosites of Arabidopsis RAF kinases in wild type, *afb1-3*, *tmk1-1*, and *abp1-TD1* mutants with or without IAA. See also Figure S6.

We next explored mechanisms of RAF activation. In time-course phosphoproteome data, we found that multiple sites on all RAF proteins are modulated upon auxin treatment (Figure 6K), suggesting profound and rapid regulation. To address which auxin binding sites might be upstream of RAF phosphorylation, we analyzed our previously recorded phosphoproteomes[19] of mutants in AUXIN BINDING PROTEIN1 (*abp1*[19]) and TRANSMEMBRANE KINASE1 (*tmk1*[19]) and generated a matched phosphoproteome of a mutant in the AUXIN F-BOX1 receptor (*afb1*). From this analysis, it emerges that RAF phosphorylation is strongly disturbed in both *abp1* and *tmk1* mutants, whereas the phosphorylation patterns on RAF proteins in the *afb1* mutant more closely resemble those in WT (Figure 6L). We therefore conclude that ABP1 and TMK1 are required for the phosphorylation of RAF-like kinases.

RAF-like kinases link rapid phospho-response to cytoplasmic streaming

We next asked if RAF-like kinases are involved in rapid cellular and physiological responses. For this, we first analyzed gravitropic root bending, as a proxy for rapid responses to endogenous auxin in Arabidopsis.[18] Gravitropic response did occur in the *raf* mutant (Figure S7A) but was subtly delayed, likely as a consequence of reduced growth rate (Figures 5F, S5C, and S5D). This suggests that RAF kinases do not play a crucial role in rapid growth responses in Arabidopsis roots. Rapid root growth responses have been connected to changes in membrane potential,[18] which we found to represent a deeply conserved auxin response (Figure 1C). We analyzed changes in membrane potential following an IAA treatment in *raf* mutant roots and compared these with *afb1* mutant as a control for which a strong effect on membrane depolarization had been reported.[18] We did not observe qualitative or quantitative changes in the *raf* mutant compared with WT (Figures 7A, 7B, S7B, and S7C). Consistently, responses to auxin treatment in membrane depolarization were normal in the Marchantia *praf* mutant (Figures 7A and 7B). We did find that Arabidopsis *raf* mutants showed an altered apoplastic root surface pH profile[81] (Figures 7C and 7D), perhaps caused by altered developmental zonation, but these displayed a WT response to IAA (Figures 7C and 7D). Therefore, consistent with the differential effect of *abp1*, *tmk1*, and *afb1* mutations of RAF phosphorylation (Figure 6L), RAF-like kinases act in a branch of auxin response distinct from AFB1. This matches the absence of TIR1/AFB1 orthologs in the algae used in phosphoproteomics and the late emergence of AFB1 in land plant evolution.[11]

In both Arabidopsis and Marchantia, *(p)raf* mutant phenotypes are characterized by reduced growth (Figures 5A–5L and S5A–S5G). Interestingly, the velocity of cytoplasmic streaming has been tightly correlated to plant organ size and organ growth. Manipulating myosin XI speed by swapping motor domains shows that the speed of the motor directly correlates with streaming velocity and plant growth.[82] Likewise, mutations in myosin XI or myosin adapter proteins reduce streaming velocity and cause growth defects similar to those in *raf* mutants.[82–84] It is therefore plausible that RAF kinases act in controlling cytoplasmic streaming. Indeed, comparing the *raf* mutant phosphoproteomes with the predicted substrates obtained from the kinase-substrate inference network (Figures S7D and S7E) identified several proteins associated with cytoplasmic streaming. These include the myosin-binding proteins MYOB1[84] and MYOB7[85] and the actin-bundling protein VILLIN4.[86]

To test the possibility that auxin-dependent acceleration of cytoplasmic streaming depends on the action of (P)RAF kinases, we examined the response of (*p*)*raf* mutants to auxin in the acceleration of cytoplasmic streaming. Strikingly, both Arabidopsis *raf* mutants and Marchantia *praf* mutants are insensitive to the promoting effect of auxin in cytoplasmic streaming (Figures 7E and 7F; Videos S3 and S4). Already in untreated Arabidopsis *raf* mutant root epidermal cells, cytoplasmic streaming is significantly reduced (Figure S7D). In Marchantia rhizoid cells, *praf* mutants showed WT cytoplasmic streaming velocity in untreated conditions, but mutant cells were insensitive to the promoting effect of auxin (Figures 7F and S7F). The response to IAA in accelerating cytoplasmic streaming in Arabidopsis was fully restored by the introduction of RAF20-sYFP and RAF24-sYFP (Figures 7E and S7F), firmly connecting RAF-like kinases to IAA-dependent cytoplasmic streaming. Collectively, we conclude that RAF proteins link rapid phosphorylation changes to a fast cellular response to auxin.

DISCUSSION

There are a number of auxin responses that are too rapid to be mediated by gene regulation, for which there is no unified mechanism yet. Second, no known mechanism can account for responses to auxin in algae, which lack the well-known transcriptional auxin response system[11,56] but demonstrate to have fast responses that are shared with land plants. After initially describing a rapid phosphorylation response to auxin in Arabidopsis roots,[19,24] we now demonstrate that auxin-triggered rapid phosphorylation-dependent signaling is conserved across the green lineage, extending beyond land plants into the streptophyte algae. We identified a key protein kinase that mediates both auxin-triggered phosphorylation and a rapid cellular response. This identifies rapid phosphorylation-dependent signaling as a mechanism that can account for both fast and deeply conserved auxin responses.

Although we compared phosphoproteomes in different tissue types and in both sporophytic (for Arabidopsis) and gametophytic tissue (for all other species), we detected a core set of functions and orthologous protein groups that are shared between all. The most parsimonious explanation is that this core set represents a truly ancient auxin "regulome" that has been retained in all these species to serve core functions. This is not trivial, given the estimated divergence times of between 500 and 850 Mya.[63] We therefore expect that further sampling of more comparable stages and tissues, such as sporophytic tissue in bryophytes, gametophyte tissue in angiosperms, or fern tissues, will extend this core set of shared phosphotargets. The sample material quantities necessary for reliable proteomic profiling are prohibitive for such comparisons, but methodological innovations in efficient tissue sampling or mass spectrometry may help overcome this limitation. In addition to the core set of phospho-targets, there are numerous lineage/clade/group/organism-specific targets. This suggests profound diversification and neofunctionalization of auxin-triggered phosphorylation pathways.

Through dense temporal phosphoproteomic profiling, we identify that Arabidopsis root cells are capable of changing the phosphorylation state of more than 1,700 proteins within 10 min of treatment with the natural auxin IAA, many of which respond within 30 s. We have not explored earlier time points, as these become technically impractical to harvest and perhaps effectivity will also be limited by the speed of IAA diffusion into roots. Computational inference suggests that the earliest responses occur around 20 s, a timeframe that is consistent with the kinetics of insulin-triggered phosphorylation in animal cells.[52] This auxin-triggered phosphorylation response is remarkably chemically specific, with natural IAA being substantially more effective than synthetic analogs, and related—but physiologically inactive—compounds being unable to trigger the response.

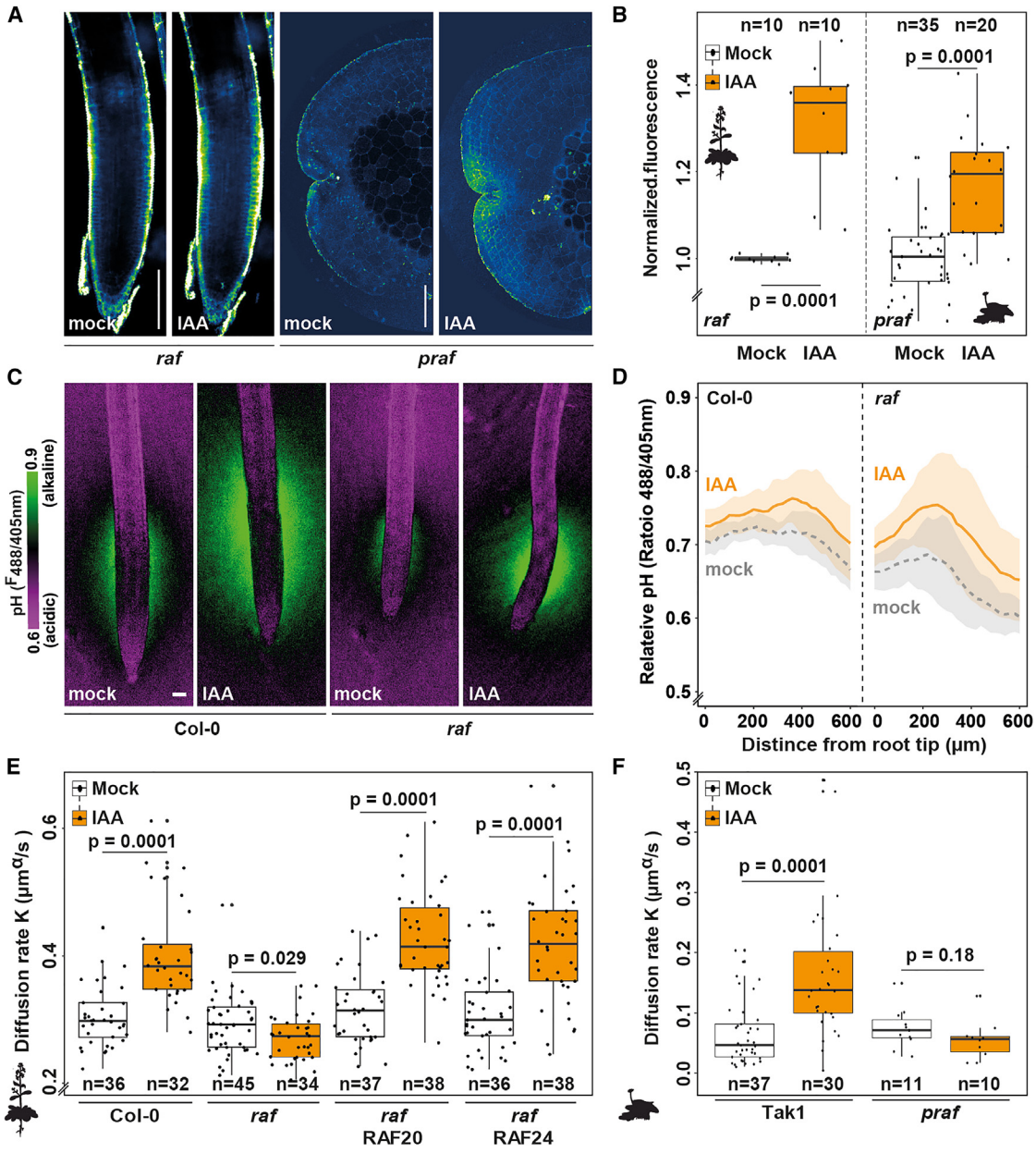

Figure 7. RAF-like kinases link phospho-response to a fast auxin response

(A and B) (A) Representative images and (B) quantification of membrane depolarization measured using DISBAC2(3) fluorescence in control (mock) and IAA-treated Arabidopsis *raf* mutant roots and Marchantia *praf* mutant rhizoid initial cells. Note that roots in (A) are the same before and after IAA treatment, and gemmae are different ones with and without IAA. Wild types for (B) are in Figure 2A. Quantification is normalized DISBAC2(3) fluorescence (IAA/mock).

(C and D) (C) Arabidopsis wild type (Col-0; n = 12 roots) and *raf* mutant (n = 11 roots) root surface pH visualized using the ratiometric pH-sensitive FS dye treated with mock or 100 nM IAA and (D) quantification of the F488/405 nm fluorescence emission ratio along the root surface. Shaded areas represent standard deviations.

(E and F) Cytoplasmic streaming in mock and IAA-treated root epidermis cells in Arabidopsis wild type (Col-0), *raf* null mutants, and *raf* mutant complemented with RAF20 or RAF24 transgenes (E) and Marchantia *praf* mutant and wild-type (Tak-1) rhizoid cells (note: the same wild-type data are shown in Figure 1F). Displayed is the diffusion rate K ($\mu m^{\alpha}/s$). Boxplots are shown along individual measurements, number of observations (n) is indicated, and significance (Student's t test) is shown. Scale bars are 100 μm (A) and 50 μm (C). See also Figure S7 and Videos S3 and S4.

The impressive dynamics of the response in Arabidopsis roots highlight a further variable that complicates comparisons between species. As IAA uptake, diffusion, inactivation, and export rates will differ between organisms (and tissues), treatments with a single concentration at a single time point are likely grossly underestimating similarities.

Through mining both comparative phosphoproteomes, kinase-substrate inference from temporal series, and motif

analysis, we identified a family of B4 RAF-like kinases (RAFs) as strong candidates for key components in the phospho-response. Exploring mutants in orthologous proteins in Arabidopsis and Marchantia, we could establish that RAF kinases are central to auxin-triggered phosphorylation and development and physiological and cellular auxin response. Curiously, transcriptional auxin responses are not impaired, which suggests that the rapid, phosphorylation-based pathway is mechanistically uncoupled from the NAP. The mutants, even in the absence of auxin treatment, have dramatic phenotypes. Although this may in part reflect altered responses to endogenous auxin, it should also be kept in mind that members of the RAF family have been implicated in responses to other triggers (e.g., light and osmotic stress).[68,74,75] Disruption of these responses likely also contributes to the strong phenotypes, and dedicated strategies will be required to deconvolute these roles.

Notably, regulation of most kinases that are differentially phosphorylated upon auxin treatment in WT Marchantia and Arabidopsis is lost in (*p*)*raf* mutants, suggesting that RAF kinases may sit at the apex of a multi-tier phosphorylation network. Interestingly, RAF kinase orthologs in mammals play an important role as master regulators of signaling cascades, for example, in EGF signaling.[87] RAF phosphorylation upon auxin treatment occurs within 30 s in Arabidopsis (the earliest sampled time point). Mammalian RAF kinases can be activated by phosphorylation within seconds to minutes after signal recognition.[88,89] Therefore, the kinetics of RAF activation is consistent with the phospho-activation of their orthologs in animal cells.

Inspired by the finding that algae and land plants share a common set of auxin phospho-targets, we explored if there were also shared cellular and physiological responses. Indeed, cytoplasmic streaming is a deeply conserved response across land plants, whereas membrane depolarization is deeply conserved across land plants and algae. Both are widespread cellular phenomena that are connected to, for example, cellular growth, nutrient distribution, and acquisition.[58,82,90] It is not clear what function the auxin-regulation of these processes serves, but analysis of these responses in *raf* mutants did help show a bifurcation of rapid auxin response mechanisms. Although auxin-dependent acceleration of cytoplasmic streaming depended on RAF, membrane depolarization did not. Interestingly, *raf* mutants already had lower streaming velocity in the absence of auxin treatment, suggesting that the same pathway operates during normal development, perhaps mediating the response to endogenous auxin.

A key question is how the auxin signal is perceived and transmitted onto RAF proteins, given that RAFs do not have a clear ligand-binding domain. Our earlier[19] and new data on phosphoproteomes in *abp1*, *tmk1*, and *afb1* mutants suggest that ABP1 and TMK1, but not AFB1, are involved in auxin signal relay to RAF. This suggests that RAFs mediate a response to apoplastic auxin. Although no clear ortholog is present in Marchantia,[91] ABP1 is a member of the large Cupin family, and other members of this family in Arabidopsis also appear to function as auxin receptors.[92] This raises the interesting possibility that the broader Cupin family, represented in all domains of life,[93] may act as auxin receptors for fast responses, including those mediated by RAF.

One striking aspect of the phosphorylation response we have discovered is that it clearly predates the origin of the nuclear auxin response pathway.[11] The nuclear auxin response did not evolve to replace this system, as the rapid response system has been retained in land plants. Thus, the rapid system likely regulates responses that the nuclear system cannot, and vice versa. One possibility is that the rapid system's primary role is to sense and respond to exogenous auxin, whereas the nuclear system mediates response to endogenous auxin. The fact that the rapid system is conserved in algal species that lack the genes that land plants use for auxin synthesis[56] would support this idea. Many organisms, including bacteria and fungi, produce and secrete auxin into their surroundings.[94–98] Given that plants and algae intimately interact with microbial communities,[99–101] we speculate that the rapid auxin response system may mediate ecological roles to exogenous auxin. The description of this response and its deep origin, and the identification of a key component, now opens avenues to genetically and biochemically characterize these pathways in the future. This will likely deepen our understanding of the origins of auxin signaling and help reveal the ancestral role of auxin within the green lineage.

Limitations of the study

A key point for future investigation is the mechanism of perception and the initial events leading to the activation of the RAF kinases. Upon binding, IAA would be expected to immediately trigger receptor activation, which one would expect to see reflected in kinase activation. With the methods used, we could not harvest tissues within 30 s, and implementation of other methods, such as microfluidics, for IAA treatment and tissue sampling could help map the very first events in this pathway.

A second question is whether the coupling of auxin phosphoreponse to RAF kinases and cellular outputs such as cytoplasmic streaming extends beyond land plants to algae. There are two main hurdles to overcome before such a connection can be made. First, imaging at high resolution in relevant streptophyte algae is technically challenging, in part due to the lack of well-established dyes or markers. Second, establishing causal connections requires genetics, including the ability to generate transgenics or mutants. Neither is possible in the algal species studied here.

Third, our results show that auxin stimulates cytoplasmic streaming and that this stimulation depends on the action of (P)RAF proteins, given that auxin treatment does not accelerate cytoplasmic streaming in *(p)raf* mutants. We can, however, neither directly demonstrate that these phenotypes are causally connected nor do we understand the molecular mechanism that links RAF kinases to cytoplasmic streaming.

A last and important future question is how the fast auxin responses connect to organismal function. One aspect is how such rapid responses translate to sustained responses, such as gene regulation. Another is what ecological or developmental contexts require such rapid signaling. Although both of these questions will require substantial efforts to be addressed, the identification of RAF kinases as key intermediaries offers a starting point to so.

STAR★METHODS

Detailed methods are provided in the online version of this paper and include the following:

- KEY RESOURCES TABLE
- RESOURCE AVAILABILITY
  - Lead contact
  - Materials availability
  - Data and code availability
- EXPERIMENTAL MODEL AND SUBJECT DETAILS
  - Plant material and culture conditions
- METHOD DETAILS
  - Generation of transgenics
  - Imaging of transgenic lines plants for RAF-localization analysis
  - Phosphoproteomics Sample preparation
  - Phosphopeptide enrichment
  - Filter-aided sample preparation and peptide fractionation
  - Mass spectrometry
  - Phosphoproteomics data analysis
  - R shiny app
  - Orthogroup construction
  - Phylogenetic analysis of RAF family
  - Cytoplasmic streaming
  - Data analysis for cytoplasmic streaming
  - Membrane potential measurement using $DISBAC_2(3)$
  - Root surface pH profile
  - Gravitropic response
  - Phenotyping
  - Transcriptomic analysis
  - RNAseq data analysis
- QUANTIFICATION AND STATISTICAL ANALYSIS

SUPPLEMENTAL INFORMATION

Supplemental information can be found online at https://doi.org/10.1016/j.cell.2023.11.021.

ACKNOWLEDGMENTS

We are grateful to Asuka Shitaku and Eri Koide for generating and sharing the Marchantia PRAF-mCitrine line and Peng-Cheng Wang for sharing the Arabidopsis *raf* mutant. We are grateful to our team members for discussions and helpful advice. This work was supported by funding from the Netherlands Organization for Scientific Research (NWO): VICI grant 865.14.001 and ENW-KLEIN OCENW.KLEIN.027 grants to D.W.; VENI grant VI.VENI.212.003 to A.K.; the European Research Council AdG DIRNDL (contract number 833867) to D.W.; CoG CATCH to J.S.; StG CELLONGATE (contract 803048) to M.F.; and AdG ETAP (contract 742985) to J.F.; MEXT KAKENHI grant number JP19H05675 to T.K.; JSPS KAKENHI grant number JP20H03275 to R.N.; Takeda Science Foundation to R.N.; and the Austrian Science Fund (FWF, P29988) to J.F.

AUTHOR CONTRIBUTIONS

Conceptualization: A.K., M.R., M.F., J.F., and D.W.; methodology: A.K., M.R., V.P.C.C., S.M., S.M.D., and J.S.; formal analysis: M.R., A.K., V.P.C.C., S.M., S.M.D., A.M., M.F., and J.S.; investigation: A.K., M.R., V.P.C.C., S.M., S.M.D., and A.M.; resources: R.N. and T.K.; writing – original draft: A.K. and D.W.; writing – review & editing: all authors; visualization: A.K., M.R., V.P.C.C., S.M., and S.M.D.; supervision: M.F., J.S., J.F., and D.W.; funding acquisition: A.K., M.F., J.F., J.S., and D.W.

DECLARATION OF INTERESTS

The authors declare no competing interests.

Received: November 25, 2022
Revised: June 29, 2023
Accepted: November 18, 2023
Published: December 20, 2023

REFERENCES

1. Friml, J. (2022). Fourteen stations of auxin. Cold Spring Harb. Perspect. Biol. *14*, a039859.
2. Friml, J., Wiśniewska, J., Benková, E., Mendgen, K., and Palme, K. (2002). Lateral relocation of auxin efflux regulator PIN3 mediates tropism in Arabidopsis. Nature *415*, 806–809.
3. Tao, Y., Ferrer, J.L., Ljung, K., Pojer, F., Hong, F., Long, J.A., Li, L., Moreno, J.E., Bowman, M.E., Ivans, L.J., et al. (2008). Rapid synthesis of auxin via a new tryptophan-dependent pathway is required for shade avoidance in plants. Cell *133*, 164–176.
4. Went, F.W., and Thimann, K.V. (1937). Phytohormones (MacMillan Company).
5. Went, F.W. (1928). Wuchsstoff und Wachstum. Recl. Trav. Bot. Neerl. *25*, 1–116.
6. Sessions, R.A., and Zambryski, P.C. (1995). Arabidopsis gynoecium structure in the wild and in ettin mutants. Development *121*, 1519–1532.
7. Nemhauser, J.L., Feldman, L.J., and Zambryski, P.C. (2000). Auxin and ETTIN in Arabidopsis gynoecium morphogenesis. Development *127*, 3877–3888.
8. Scarpella, E., Marcos, D., Friml, J., and Berleth, T. (2006). Control of leaf vascular patterning by polar auxin transport. Genes Dev. *20*, 1015–1027.
9. De Rybel, B., Adibi, M., Breda, A.S., Wendrich, J.R., Smit, M.E., Novák, O., Yamaguchi, N., Yoshida, S., Van Isterdael, G., Palovaara, J., et al. (2014). Plant development. Integration of growth and patterning during vascular tissue formation in *Arabidopsis*. Science *345*, 1255215.
10. Morffy, N., and Strader, L.C. (2020). Old Town Roads: routes of auxin biosynthesis across kingdoms. Curr. Opin. Plant Biol. *55*, 21–27.
11. Mutte, S.K., Kato, H., Rothfels, C., Melkonian, M., Wong, G.K.-S., and Weijers, D. (2018). Origin and evolution of the nuclear auxin response system. eLife *7*, e33399.
12. Jin, Q., Scherp, P., Heimann, K., and Hasenstein, K.H. (2008). Auxin and cytoskeletal organization in algae. Cell Biol. Int. *32*, 542–545.
13. Ohtaka, K., Hori, K., Kanno, Y., Seo, M., and Ohta, H. (2017). Primitive auxin response without TIR1 and aux/IAA in the charophyte alga *Klebsormidium nitens*. Plant Physiol. *174*, 1621–1632.
14. Klämbt, D., Knauth, B., and Dittmann, I. (1992). Auxin dependent growth of rhizoids of Chara globularis. Physiol. Plant. *85*, 537–540.
15. Wood, N.L., and Berliner, M.D. (1979). Effects of indoleacetic acid on the desmid Micrasterias thomasiana. Plant Sci. Lett. *16*, 285–289.
16. Etherton, B. (1970). Effect of indole-3-acetic acid on membrane potentials of oat coleoptile cells. Plant Physiol. *45*, 527–528.
17. Bates, G.W., and Goldsmith, M.H.M. (1983). Rapid response of the plasma-membrane potential in oat coleoptiles to auxin and other weak acids. Planta *159*, 231–237.
18. Serre, N.B.C., Kralík, D., Yun, P., Slouka, Z., Shabala, S., and Fendrych, M. (2021). AFB1 controls rapid auxin signalling through membrane depolarization in Arabidopsis thaliana root. Nat. Plants *7*, 1229–1238.
19. Friml, J., Gallei, M., Gelová, Z., Johnson, A., Mazur, E., Monzer, A., Rodriguez, L., Roosjen, M., Verstraeten, I., Živanović, B.D., et al. (2022).

ABP1–TMK auxin perception for global phosphorylation and auxin canalization. Nature *609*, 575–581.

20. Ayling, S., and Clarkson, D. (1996). The cytoplasmic streaming response of tomato root hairs to auxin; the role of calcium. Funct. Plant Biol. *23*, 699.
21. Monshausen, G.B., Miller, N.D., Murphy, A.S., and Gilroy, S. (2011). Dynamics of auxin-dependent Ca2+ and pH signaling in root growth revealed by integrating high-resolution imaging with automated computer vision-based analysis. Plant J. *65*, 309–318.
22. Barbez, E., Dünser, K., Gaidora, A., Lendl, T., and Busch, W. (2017). Auxin steers root cell expansion via apoplastic pH regulation in *Arabidopsis thaliana*. Proc. Natl. Acad. Sci. USA *114*, E4884–E4893.
23. Shih, H.W., DePew, C.L., Miller, N.D., and Monshausen, G.B. (2015). The cyclic nucleotide-gated channel CNGC14 regulates root gravitropism in Arabidopsis thaliana. Curr. Biol. *25*, 3119–3125.
24. Li, L., Verstraeten, I., Roosjen, M., Takahashi, K., Rodriguez, L., Merrin, J., Chen, J., Shabala, L., Smet, W., Ren, H., et al. (2021). Cell surface and intracellular auxin signalling for H+ fluxes in root growth. Nature *599*, 273–277.
25. Senn, A.P., and Goldsmith, M.H.M. (1988). Regulation of electrogenic proton pumping by auxin and fusicoccin as related to the growth of *Avena* coleoptiles. Plant Physiol. *88*, 131–138.
26. Narasimhan, M., Gallei, M., Tan, S., Johnson, A., Verstraeten, I., Li, L., Rodriguez, L., Han, H., Himschoot, E., Wang, R., et al. (2021). Systematic analysis of specific and nonspecific auxin effects on endocytosis and trafficking. Plant Physiol. *186*, 1122–1142.
27. Heisler, M.G., Ohno, C., Das, P., Sieber, P., Reddy, G.V., Long, J.A., and Meyerowitz, E.M. (2005). Patterns of auxin transport and gene expression during primordium development revealed by live imaging of the Arabidopsis inflorescence meristem. Curr. Biol. *15*, 1899–1911.
28. Dubrovsky, J.G., Sauer, M., Napsucialy-Mendivil, S., Ivanchenko, M.G., Friml, J., Shishkova, S., Celenza, J., and Benková, E. (2008). Auxin acts as a local morphogenetic trigger to specify lateral root founder cells. Proc. Natl. Acad. Sci. USA *105*, 8790–8794.
29. Reinhardt, D., Pesce, E.R., Stieger, P., Mandel, T., Baltensperger, K., Bennett, M., Traas, J., Friml, J., and Kuhlemeier, C. (2003). Regulation of phyllotaxis by polar auxin transport. Nature *426*, 255–260.
30. Thimann, K.V. (1938). Hormones and the analysis of growth. Plant Physiol. *13*, 437–449.
31. Kepinski, S., and Leyser, O. (2005). The Arabidopsis F-box protein TIR1 is an auxin receptor. Nature *435*, 446–451.
32. Dharmasiri, N., Dharmasiri, S., and Estelle, M. (2005). The F-box protein TIR1 is an auxin receptor. Nature *435*, 441–445.
33. Tan, X., Calderon-Villalobos, L.I.A., Sharon, M., Zheng, C., Robinson, C.V., Estelle, M., and Zheng, N. (2007). Mechanism of auxin perception by the TIR1 ubiquitin ligase. Nature *446*, 640–645.
34. Gray, W.M., Kepinski, S., Rouse, D., Leyser, O., and Estelle, M. (2001). Auxin regulates SCF(TIR1)-dependent degradation of AUX/IAA proteins. Nature *414*, 271–276.
35. Kim, J., Harter, K., and Theologis, A. (1997). Protein–protein interactions among the Aux/IAA proteins. Proc. Natl. Acad. Sci. USA *94*, 11786–11791.
36. Weijers, D., and Wagner, D. (2016). Transcriptional responses to the auxin hormone. Annu. Rev. Plant Biol. *67*, 539–574.
37. Prigge, M.J., Platre, M., Kadakia, N., Zhang, Y., Greenham, K., Szutu, W., Pandey, B.K., Bhosale, R.A., Bennett, M.J., Busch, W., et al. (2020). Genetic analysis of the Arabidopsis TIR1/AFB auxin receptors reveals both overlapping and specialized functions. eLife *9*, e54740.
38. Hamann, T., Benkova, E., Bäurle, I., Kientz, M., and Jürgens, G. (2002). The *Arabidopsis BODENLOS* gene encodes an auxin response protein inhibiting MONOPTEROS-mediated embryo patterning. Genes Dev. *16*, 1610–1615.
39. Hardtke, C.S., and Berleth, T. (1998). The Arabidopsis gene MONOPTEROS encodes a transcription factor mediating embryo axis formation and vascular development. EMBO J. *17*, 1405–1411.
40. Kato, H., Mutte, S.K., Suzuki, H., Crespo, I., Das, S., Radoeva, T., Fontana, M., Yoshitake, Y., Hainiwa, E., van den Berg, W., et al. (2020). Design principles of a minimal auxin response system. Nat. Plants *6*, 473–482.
41. Abel, S., and Theologis, A. (1996). Early genes and auxin action. Plant Physiol. *111*, 9–17.
42. McClure, B.A., Hagen, G., Brown, C.S., Gee, M.A., and Guilfoyle, T.J. (1989). Transcription, organization, and sequence of an auxin-regulated gene cluster in soybean. Plant Cell *1*, 229–239.
43. Fendrych, M., Akhmanova, M., Merrin, J., Glanc, M., Hagihara, S., Takahashi, K., Uchida, N., Torii, K.U., and Friml, J. (2018). Rapid and reversible root growth inhibition by TIR1 auxin signalling. Nat. Plants *4*, 453–459.
44. Dindas, J., Scherzer, S., Roelfsema, M.R.G., von Meyer, K., Müller, H.M., Al-Rasheid, K.A.S., Palme, K., Dietrich, P., Becker, D., Bennett, M.J., et al. (2018). AUX1-mediated root hair auxin influx governs SCFTIR1/AFB-type Ca2+ signaling. Nat. Commun. *9*, 1174.
45. Serre, N.B., Wernerova, D., Vittal, P., Dubey, S.M., Medvecka, E., Jelinkova, A., Petrasek, J., Grossmann, G., and Fendrych, M. (2023). The AUX1-AFB1-CNGC14 module establishes longitudinal root surface pH profile. Elife *12*, e85193.
46. Dubey, S.M., Han, S., Stutzman, N., Prigge, M.J., Medvecká, E., Platre, M.P., Busch, W., Fendrych, M., and Estelle, M. (2023). The AFB1 auxin receptor controls the cytoplasmic auxin response pathway in Arabidopsis thaliana. Mol. Plant. *16*, 1120–1130.
47. Qi, L., Kwiatkowski, M., Chen, H., Hoermayer, L., Sinclair, S., Zou, M., del Genio, C.I., Kubeš, M.F., Napier, R., Jaworski, K., et al. (2022). Adenylate cyclase activity of TIR1/AFB auxin receptors in plants. Nature *611*, 133–138.
48. Jin, J., and Pawson, T. (2012). Modular evolution of phosphorylation-based signalling systems. Philos. Trans. R. Soc. Lond. B Biol. Sci. *367*, 2540–2555.
49. Nürnberger, T., Brunner, F., Kemmerling, B., and Piater, L. (2004). Innate immunity in plants and animals: striking similarities and obvious differences. Immunol. Rev. *198*, 249–266.
50. Couto, D., and Zipfel, C. (2016). Regulation of pattern recognition receptor signalling in plants. Nat. Rev. Immunol. *16*, 537–552.
51. Oyama, M., Kozuka-Hata, H., Tasaki, S., Semba, K., Hattori, S., Sugano, S., Inoue, J., and Yamamoto, T. (2009). Temporal perturbation of tyrosine phosphoproteome dynamics reveals the system-wide regulatory networks. Mol. Cell. Proteomics *8*, 226–231.
52. Humphrey, S.J., Azimifar, S.B., and Mann, M. (2015). High-throughput phosphoproteomics reveals in vivo insulin signaling dynamics. Nat. Biotechnol. *33*, 990–995.
53. Kinoshita, T., Caño-Delgado, A., Seto, H., Hiranuma, S., Fujioka, S., Yoshida, S., and Chory, J. (2005). Binding of brassinosteroids to the extracellular domain of plant receptor kinase BRI1. Nature *433*, 167–171.
54. Wang, X., Kota, U., He, K., Blackburn, K., Li, J., Goshe, M.B., Huber, S.C., and Clouse, S.D. (2008). Sequential transphosphorylation of the BRI1/BAK1 receptor kinase complex impacts early events in brassinosteroid signaling. Dev. Cell *15*, 220–235.
55. Ryu, H., Kim, K., Cho, H., Park, J., Choe, S., and Hwang, I. (2007). Nucleocytoplasmic shuttling of BZR1 mediated by phosphorylation is essential in *Arabidopsis* brassinosteroid signaling. Plant Cell *19*, 2749–2762.
56. Carrillo-Carrasco, V.P., Hernandez-Garcia, J., Mutte, S.K., and Weijers, D. (2023). The birth of a giant: evolutionary insights into the origin of auxin responses in plants. EMBO J. *42*, e113018.
57. Ren, H., Park, M.Y., Spartz, A.K., Wong, J.H., and Gray, W.M. (2018). A subset of plasma membrane-localized PP2C.D phosphatases negatively regulate SAUR-mediated cell expansion in Arabidopsis. PLoS Genet. *14*, e1007455.

58. Takahashi, K., Hayashi, K., and Kinoshita, T. (2012). Auxin activates the plasma membrane H+-ATPase by phosphorylation during hypocotyl elongation in Arabidopsis. Plant Physiol. *159*, 632–641.

59. Renier, M., Tamanini, A., Nicolis, E., Rolfini, R., Imler, J.L., Pavirani, A., and Cabrini, G. (1995). Use of a membrane potential-sensitive probe to assess biological expression of the cystic fibrosis transmembrane conductance regulator. Hum. Gene Ther. *6*, 1275–1283.

60. Tominaga, M., and Ito, K. (2015). The molecular mechanism and physiological role of cytoplasmic streaming. Curr. Opin. Plant Biol. *27*, 104–110.

61. Metzler, R., Jeon, J.H., Cherstvy, A.G., and Barkai, E. (2014). Anomalous diffusion models and their properties: non-stationarity, non-ergodicity, and ageing at the centenary of single particle tracking. Phys. Chem. Chem. Phys. *16*, 24128–24164.

62. Regner, B.M., Vučinić, D., Domnisoru, C., Bartol, T.M., Hetzer, M.W., Tartakovsky, D.M., and Sejnowski, T.J. (2013). Anomalous diffusion of single particles in cytoplasm. Biophys. J. *104*, 1652–1660.

63. Yoon, H.S., Hackett, J.D., Ciniglia, C., Pinto, G., and Bhattacharya, D. (2004). A molecular timeline for the origin of photosynthetic eukaryotes. Mol. Biol. Evol. *21*, 809–818.

64. One Thousand Plant Transcriptomes Initiative (2019). One thousand plant transcriptomes and the phylogenomics of green plants. Nature *574*, 679–685.

65. Jiao, C., Sørensen, I., Sun, X., Sun, H., Behar, H., Alseekh, S., Philippe, G., Palacio Lopez, K., Sun, L., Reed, R., et al. (2020). The Penium margaritaceum genome: hallmarks of the origins of land plants. Cell *181*, 1097–1111.e12.

66. Kaur, S., Peters, T.J., Yang, P., Luu, L.D.W., Vuong, J., Krycer, J.R., and O'Donoghue, S.I. (2020). Temporal ordering of omics and multiomic events inferred from time-series data. NPJ Syst. Biol. Appl. *6*, 22.

67. Montes, C., Wang, P., Liao, C.Y., Nolan, T.M., Song, G., Clark, N.M., Elmore, J.M., Guo, H., Bassham, D.C., Yin, Y., et al. (2022). Integration of multi-omics data reveals interplay between brassinosteroid and target of rapamycin complex signaling in Arabidopsis. New Phytol. *236*, 893–910.

68. Lin, Z., Li, Y., Zhang, Z., Liu, X., Hsu, C.C., Du, Y., Sang, T., Zhu, C., Wang, Y., Satheesh, V., et al. (2020). A RAF-SnRK2 kinase cascade mediates early osmotic stress signaling in higher plants. Nat. Commun. *11*, 613.

69. Sirichandra, C., Davanture, M., Turk, B.E., Zivy, M., Valot, B., Leung, J., and Merlot, S. (2010). The Arabidopsis ABA-activated kinase OST1 phosphorylates the bZIP transcription factor ABF3 and creates a 14-3-3 Binding Site involved in its turnover. PLoS One *5*, e13935.

70. Weller, B., Zourelidou, M., Frank, L., Barbosa, I.C.R., Fastner, A., Richter, S., Jürgens, G., Hammes, U.Z., and Schwechheimer, C. (2017). Dynamic PIN-FORMED auxin efflux carrier phosphorylation at the plasma membrane controls auxin efflux-dependent growth. Proc. Natl. Acad. Sci. USA *114*, E887–E896.

71. Songyang, Z., Lu, K.P., Kwon, Y.T., Tsai, L.H., Filhol, O., Cochet, C., Brickey, D.A., Soderling, T.R., Bartleson, C., Graves, D.J., et al. (1996). A structural basis for substrate specificities of protein Ser/Thr kinases: primary sequence preference of casein kinases I and II, NIMA, phosphorylase kinase, calmodulin-dependent kinase II, CDK5, and Erk1. Mol. Cell. Biol. *16*, 6486–6493.

72. Lewis, T.S., Shapiro, P.S., and Ahn, N.G. (1998). Signal transduction through MAP kinase cascades. Adv. Cancer Res. *74*, 49–139.

73. Ichimura, K., Ichimura, K., Shinozaki, K., Tena, G., Sheen, J., Henry, Y., Champion, A., Kreis, M., Zhang, S., Hirt, H., et al. (2002). Mitogen-activated protein kinase cascades in plants: a new nomenclature. Trends Plant Sci. *7*, 301–308.

74. Shahzad, Z., Canut, M., Tournaire-Roux, C., Martinière, A., Boursiac, Y., Loudet, O., and Maurel, C. (2016). A potassium-dependent oxygen sensing pathway regulates plant root hydraulics. Cell *167*, 87–98.e14.

75. Koide, E., Suetsugu, N., Iwano, M., Gotoh, E., Nomura, Y., Stolze, S.C., Nakagami, H., Kohchi, T., and Nishihama, R. (2020). Regulation of photosynthetic carbohydrate metabolism by a Raf-like kinase in the liverwort Marchantia polymorpha. Plant Cell Physiol. *61*, 631–643.

76. Bowman, J.L., Kohchi, T., Yamato, K.T., Jenkins, J., Shu, S., Ishizaki, K., Yamaoka, S., Nishihama, R., Nakamura, Y., Berger, F., et al. (2017). Insights into land plant evolution garnered from the Marchantia polymorpha genome. Cell *171*, 287–304.e15.

77. Bienz, M. (2014). Signalosome assembly by domains undergoing dynamic head-to-tail polymerization. Trends Biochem. Sci. *39*, 487–495.

78. Benková, E., Michniewicz, M., Sauer, M., Teichmann, T., Seifertová, D., Jürgens, G., and Friml, J. (2003). Local, efflux-dependent auxin gradients as a common module for plant organ formation. Cell *115*, 591–602.

79. Flores-Sandoval, E., Eklund, D.M., and Bowman, J.L. (2015). A simple auxin transcriptional response system regulates multiple morphogenetic processes in the liverwort Marchantia polymorpha. PLoS Genet. *11*, e1005207.

80. Soma, F., Takahashi, F., Suzuki, T., Shinozaki, K., and Yamaguchi-Shinozaki, K. (2020). Plant Raf-like kinases regulate the mRNA population upstream of ABA-unresponsive SnRK2 kinases under drought stress. Nat. Commun. *11*, 1373.

81. Serre, N.B.C., Wernerová, D., Vittal, P., Dubey, S.M., Medvecká, E., Jelínková, A., Petrášek, J., Grossmann, G., and Fendrych, M. (2023). The AUX1-AFB1-CNGC14 module establishes a longitudinal root surface pH profile. eLife *12*, e85193.

82. Tominaga, M., Kimura, A., Yokota, E., Haraguchi, T., Shimmen, T., Yamamoto, K., Nakano, A., and Ito, K. (2013). Cytoplasmic streaming velocity as a plant size determinant. Dev. Cell *27*, 345–352.

83. Prokhnevsky, A.I., Peremyslov, V.V., and Dolja, V.V. (2008). Overlapping functions of the four class XI myosins in Arabidopsis growth, root hair elongation, and organelle motility. Proc. Natl. Acad. Sci. USA *105*, 19744–19749.

84. Peremyslov, V.V., Cole, R.A., Fowler, J.E., and Dolja, V.V. (2015). Myosin-powered membrane compartment drives cytoplasmic streaming, cell expansion and plant development. PLoS One *10*, e0139331.

85. Kurth, E.G., Peremyslov, V.V., Turner, H.L., Makarova, K.S., Iranzo, J., Mekhedov, S.L., Koonin, E.V., and Dolja, V.V. (2017). Myosin-driven transport network in plants. Proc. Natl. Acad. Sci. USA *114*, E1385–E1394.

86. Zhang, Y., Xiao, Y., Du, F., Cao, L., Dong, H., and Ren, H. (2011). Arabidopsis VILLIN4 is involved in root hair growth through regulating actin organization in a Ca^{2+}-dependent manner. New Phytol. *190*, 667–682.

87. Moscat, J., Diaz-Meco, M.T., Albert, A., and Campuzano, S. (2006). Cell signaling and function organized by PB1 domain interactions. Mol. Cell *23*, 631–640.

88. Blagoev, B., Ong, S.E., Kratchmarova, I., and Mann, M. (2004). Temporal analysis of phosphotyrosine-dependent signaling networks by quantitative proteomics. Nat. Biotechnol. *22*, 1139–1145.

89. Winston, B.W., Lange-Carter, C.A., Gardner, A.M., Johnson, G.L., and Riches, D.W. (1995). Tumor necrosis factor alpha rapidly activates the mitogen-activated protein kinase (MAPK) cascade in a MAPK kinase kinase-dependent, c-Raf-1-independent fashion in mouse macrophages. Proc. Natl. Acad. Sci. USA *92*, 1614–1618.

90. Du, M., Spalding, E.P., and Gray, W.M. (2020). Rapid auxin-mediated cell expansion. Annu. Rev. Plant Biol. *71*, 379–402.

91. Kato, H., Ishizaki, K., Kouno, M., Shirakawa, M., Bowman, J.L., Nishihama, R., and Kohchi, T. (2015). Auxin-mediated transcriptional system with a minimal set of components is critical for morphogenesis through the life cycle in Marchantia polymorpha. PLoS Genet. *11*, e1005084.

92. Yu, Y., Tang, W., Lin, W., Li, W., Zhou, X., Li, Y., Chen, R., Zheng, R., Qin, G., Cao, W., et al. (2023). ABLs and TMKs are co-receptors for extracellular auxin. Cell *186*, 5457–5471.

93. Khuri, S., Bakker, F.T., and Dunwell, J.M. (2001). Phylogeny, function, and evolution of the cupins, a structurally conserved, functionally diverse superfamily of proteins. Mol. Biol. Evol. *18*, 593–605.

94. Leontovyčová, H., Trdá, L., Dobrev, P.I., Šašek, V., Gay, E., Balesdent, M.H., and Burketová, L. (2020). Auxin biosynthesis in the phytopathogenic fungus Leptosphaeria maculans is associated with enhanced transcription of indole-3-pyruvate decarboxylase LmIPDC2 and tryptophan aminotransferase LmTAM1. Res. Microbiol. *171*, 174–184.

95. Cox, C.E., Brandl, M.T., de Moraes, M.H., Gunasekera, S., and Teplitski, M. (2017). Production of the plant hormone auxin by Salmonella and its role in the interactions with plants and animals. Front. Microbiol. *8*, 2668.

96. Chanclud, E., and Morel, J.B. (2016). Plant hormones: a fungal point of view. Mol. Plant Pathol. *17*, 1289–1297.

97. Rao, R.P., Hunter, A., Kashpur, O., and Normanly, J. (2010). Aberrant synthesis of indole-3-acetic acid in Saccharomyces cerevisiae triggers morphogenic transition, a virulence trait of pathogenic fungi. Genetics *185*, 211–220.

98. Le Bail, A., Billoud, B., Kowalczyk, N., Kowalczyk, M., Gicquel, M., Le Panse, S., Stewart, S., Scornet, D., Cock, J.M., Ljung, K., et al. (2010). Auxin metabolism and function in the multicellular brown alga Ectocarpus siliculosus. Plant Physiol. *153*, 128–144.

99. Kunkel, B.N., and Harper, C.P. (2018). The roles of auxin during interactions between bacterial plant pathogens and their hosts. J. Exp. Bot. *69*, 245–254.

100. Stringlis, I.A., Proietti, S., Hickman, R., Van Verk, M.C., Zamioudis, C., and Pieterse, C.M.J. (2018). Root transcriptional dynamics induced by beneficial rhizobacteria and microbial immune elicitors reveal signatures of adaptation to mutualists. Plant J. *93*, 166–180.

101. Amin, S.A., Hmelo, L.R., van Tol, H.M., Durham, B.P., Carlson, L.T., Heal, K.R., Morales, R.L., Berthiaume, C.T., Parker, M.S., Djunaedi, B., et al. (2015). Interaction and signalling between a cosmopolitan phytoplankton and associated bacteria. Nature *522*, 98–101.

102. Koncz, C., and Schell, J. (1986). The promoter of TL-DNA gene 5 controls the tissue-specific expression of chimaeric genes carried by a novel type of Agrobacterium binary vector. Mol. Gen. Genet. *204*, 383–396.

103. Deblaere, R., Bytebier, B., De Greve, H., Deboeck, F., Schell, J., Van Montagu, M., and Leemans, J. (1985). Efficient octopine Ti plasmid-derived vectors for *Agrobacterium* -mediated gene transfer to plants. Nucleic Acids Res. *13*, 4777–4788.

104. Nishiyama, T., Hiwatashi, Y., Sakakibara, I., Kato, M., and Hasebe, M. (2000). Tagged mutagenesis and gene-trap in the moss, Physcomitrella patens by shuttle mutagenesis. DNA Res. *7*, 9–17.

105. Domozych, D.S., Sørensen, I., Popper, Z.A., Ochs, J., Andreas, A., Fangel, J.U., Pielach, A., Sacks, C., Brechka, H., Ruisi-Besares, P., et al. (2014). Pectin metabolism and assembly in the cell wall of the charophyte green alga Penium margaritaceum. Plant Physiol. *165*, 105–118.

106. Ishizaki, K., Chiyoda, S., Yamato, K.T., and Kohchi, T. (2008). Agrobacterium-mediated transformation of the haploid liverwort Marchantia polymorpha L., an emerging model for plant biology. Plant Cell Physiol. *49*, 1084–1091.

107. Ashton, N.W., and Cove, D.J. (1977). The isolation and preliminary characterisation of auxotrophic and analogue resistant mutants of the moss, Physcomitrella patens. Mol. Gen. Genet. *154*, 87–95.

108. Savaldi-Goldstein, S., Baiga, T.J., Pojer, F., Dabi, T., Butterfield, C., Parry, G., Santner, A., Dharmasiri, N., Tao, Y., Estelle, M., et al. (2008). New auxin analogs with growth-promoting effects in intact plants reveal a chemical strategy to improve hormone delivery. Proc. Natl. Acad. Sci. USA *105*, 15190–15195.

109. De Rybel, B., van den Berg, W., Lokerse, A.S., Liao, C.Y., van Mourik, H., Möller, B., Peris, C.L., and Weijers, D. (2011). A versatile set of ligation-independent cloning vectors for functional studies in plants. Plant Physiol. *156*, 1292–1299.

110. Ishizaki, K., Nishihama, R., Ueda, M., Inoue, K., Ishida, S., Nishimura, Y., Shikanai, T., and Kohchi, T. (2015). Development of gateway binary vector series with four different selection markers for the liverwort Marchantia polymorpha. PLoS One *10*, e0138876.

111. Tyanova, S., Temu, T., and Cox, J. (2016). The MaxQuant computational platform for mass spectrometry-based shotgun proteomics. Nat. Protoc. *11*, 2301–2319.

112. Tyanova, S., Temu, T., Sinitcyn, P., Carlson, A., Hein, M.Y., Geiger, T., Mann, M., and Cox, J. (2016). The Perseus computational platform for comprehensive analysis of (prote)omics data. Nat. Methods *13*, 731–740.

113. Sherman, B.T., Hao, M., Qiu, J., Jiao, X., Baseler, M.W., Lane, H.C., Imamichi, T., and Chang, W. (2022). DAVID: a web server for functional enrichment analysis and functional annotation of gene lists (2021 update). Nucleic Acids Res. *50*, W216–W221.

114. Supek, F., Bošnjak, M., Škunca, N., and Šmuc, T. (2011). REVIGO summarizes and visualizes long lists of gene ontology terms. PLoS One *6*, e21800.

115. Shannon, P., Markiel, A., Ozier, O., Baliga, N.S., Wang, J.T., Ramage, D., Amin, N., Schwikowski, B., and Ideker, T. (2003). Cytoscape: a software environment for integrated models of biomolecular interaction networks. Genome Res. *13*, 2498–2504.

116. Jumper, J., Evans, R., Pritzel, A., Green, T., Figurnov, M., Ronneberger, O., Tunyasuvunakool, K., Bates, R., Žídek, A., Potapenko, A., et al. (2021). Highly accurate protein structure prediction with AlphaFold. Nature *596*, 583–589.

117. Emms, D.M., and Kelly, S. (2019). OrthoFinder: phylogenetic orthology inference for comparative genomics. Genome Biol. *20*, 238.

118. Serre, N.B.C., and Fendrych, M. (2022). ACORBA: automated workflow to measure *Arabidopsis thaliana* root tip angle dynamics. Quant. Plant Biol. *3*, e9.

119. Schindelin, J., Arganda-Carreras, I., Frise, E., Kaynig, V., Longair, M., Pietzsch, T., Preibisch, S., Rueden, C., Saalfeld, S., Schmid, B., et al. (2012). Fiji: an open-source platform for biological-image analysis. Nat. Methods *9*, 676–682.

120. Kim, D., Langmead, B., and Salzberg, S.L. (2015). HISAT: a fast spliced aligner with low memory requirements. Nat. Methods *12*, 357–360.

121. Danecek, P., Bonfield, J.K., Liddle, J., Marshall, J., Ohan, V., Pollard, M.O., Whitwham, A., Keane, T., McCarthy, S.A., Davies, R.M., et al. (2021). Twelve years of SAMtools and BCFtools. GigaScience *10*, giab008.

122. Liao, Y., Smyth, G.K., and Shi, W. (2014). featureCounts: an efficient general purpose program for assigning sequence reads to genomic features. Bioinformatics *30*, 923–930.

123. Love, M.I., Huber, W., and Anders, S. (2014). Moderated estimation of fold change and dispersion for RNA-seq data with DESeq2. Genome Biol. *15*, 550.

124. Nakamura, T., Yamada, K.D., Tomii, K., and Katoh, K. (2018). Parallelization of MAFFT for large-scale multiple sequence alignments. Bioinformatics *34*, 2490–2492.

125. Kalyaanamoorthy, S., Minh, B.Q., Wong, T.K.F., von Haeseler, A., and Jermiin, L.S. (2017). ModelFinder: fast model selection for accurate phylogenetic estimates. Nat. Methods *14*, 587–589.

126. Hoang, D.T., Chernomor, O., von Haeseler, A., Minh, B.Q., and Vinh, L.S. (2018). UFBoot2: improving the ultrafast bootstrap approximation. Mol. Biol. Evol. *35*, 518–522.

127. Murashige, T., and Skoog, F. (1962). A revised medium for rapid growth and bio assays with tobacco tissue cultures. Physiol. Plant. *15*, 473–497.

128. Gamborg, O.L., Miller, R.A., and Ojima, K. (1968). Nutrient requirements of suspension cultures of soybean root cells. Exp. Cell Res. *50*, 151–158.

129. Cove, D.J., Perroud, P.F., Charron, A.J., McDaniel, S.F., Khandelwal, A., and Quatrano, R.S. (2009). Culturing the moss Physcomitrella patens. Cold Spring Harb. Protoc. *2009*, pdb.prot5136.

130. Kubota, A., Ishizaki, K., Hosaka, M., and Kohchi, T. (2013). Efficient Agrobacterium-mediated transformation of the liverwort Marchantia polymorpha using regenerating thalli. Biosci. Biotechnol. Biochem. *77*, 167–172.

131. Huang, D.W., Sherman, B.T., and Lempicki, R.A. (2009). Systematic and integrative analysis of large gene lists using DAVID bioinformatics resources. Nat. Protoc. *4*, 44–57.

132. Capella-Gutiérrez, S., Silla-Martínez, J.M., and Gabaldón, T. (2009). trimAl: a tool for automated alignment trimming in large-scale phylogenetic analyses. Bioinformatics *25*, 1972–1973.

133. Letunic, I., and Bork, P. (2021). Interactive Tree Of Life (iTOL) v5: an online tool for phylogenetic tree display and annotation. Nucleic Acids Res. *49*, W293–W296.

134. Gao, Y., and Kilfoil, M.L. (2009). Accurate detection and complete tracking of large populations of features in three dimensions. Opt. Express *17*, 4685–4704.

135. Cheng, C.Y., Krishnakumar, V., Chan, A.P., Thibaud-Nissen, F., Schobel, S., and Town, C.D. (2017). Araport11: a complete reannotation of the *Arabidopsis thaliana* reference genome. Plant J. *89*, 789–804.

136. Montgomery, S.A., Tanizawa, Y., Galik, B., Wang, N., Ito, T., Mochizuki, T., Akimcheva, S., Bowman, J.L., Cognat, V., Maréchal-Drouard, L., et al. (2020). Chromatin organization in early land plants reveals an ancestral association between H3K27me3, transposons, and constitutive heterochromatin. Curr. Biol. *30*, 573–588.e7.

137. Li, H., Handsaker, B., Wysoker, A., Fennell, T., Ruan, J., Homer, N., Marth, G., Abecasis, G., and Durbin, R.; 1000 Genome Project Data Processing Subgroup (2009). The Sequence Alignment/Map format and SAMtools. Bioinformatics *25*, 2078–2079.

STAR★METHODS

KEY RESOURCES TABLE

REAGENT or RESOURCE	SOURCE	IDENTIFIER
Bacterial and virus strains		
Escherichia coli DH5a	Widely distributed	N/A
Agrobacterium tumefaciens GV3101	Koncz and Schell[102]	N/A
Agrobacterium tumefaciens GV2260	Deblaere et al.[103]	N/A
Chemicals, peptides, and recombinant proteins		
Murashige and Skoog (MS) medium	Duchefa	Cat#: M0221
Gamborg's B5 salts	Duchefa	Cat#: G0209
BCD medium	Nishiyama et al.[104]	N/A
Kanamycin sulphate monohydrate	Duchefa	Cat#: K0126
Woods Hole Medium (WHM)	Domozych et al.[105]	N/A
NEBuilder HiFi DNA Assembly Master Mix	BIOKE	Cat#: E2621X
BsaI-HF v2	BIOKE	Cat#: R3733L
In-Fusion HD Cloning Kit	TaKaRa Bio	Cat#: 102518
pENTR/D-TOPO Cloning Kit	Thermo Fisher Scientific	Cat#: K2400-20
FASTDIGEST HINDIII 800UL	Thermo Fisher Scientific	Cat#: FD0504
SACI-HF	BIOKE	Cat#: R3156L
Dimethyl sulfoxide (DMSO)	Thermo Fisher Scientific	Cat#: 022914.K2
Indole-3-Actetic Acid (IAA)	AlfaAesar	Cat#: A10556
1-Naphthaleneacetic acid (1-NAA)	Sigma	Cat#: N0640
2-Naphthaleneacetic acid (2-NAA)	Sigma	Cat#: N4002
2,4-Dichlorophenoxyacetic acid (2,4-D)	Sigma	Cat#: D70724
Formic Acid	Merck	Cat#: 695076
Benzoic Acid	AlfaAesar	Cat#: 036230.22
Triton-X 100	Sigma	Cat#: T8787
Dithiothreitol (DTT)	Duchefa	Cat#: D1309
DNAseI	Roche	Cat#: 10104159001
Benzonase 90% Purity	Novagen	Cat#: 70664-3
Acrylamide	Merck	Cat#: 8008300100
NP-40	AppliChem	Cat#: A1694
Methanol	VWR Chemicals	Cat#: 20863.320
Chloroform	Honeywell Riedel-de Haen	Cat#: 34854
Ammonium Bicarbonate	Sigma	Cat#: 09830
Bradford reagent	Biorad	Cat#: 5000006
Trypsin (sequencing grade)	Merck	Cat#: 11047841001
SPE Disk C18 octadecyl 47 mm	Empore	Cat#: 66883-U
LiChroprep® RP-18	Merck	Cat#: 1093030100
Acetonitrile	VWR Chemicals	Cat#: 20060.320
Tri-Fluor Acetic acid (TFA)	AlfaAesar	Cat#: 44630
MagReSyn® Ti-IMAC beads	Resyn bioscience	Cat#: MR-TIM010
Amicon Ultra centrifugal filter units, Ultra-4 (30kDa cut off)	Merck Millipore	Cat#: UFC8100
Ammonium Formate	Optima	A11550
Rhodamine123	Thermo Fisher Scientific	Cat#: R302

(*Continued on next page*)

Continued

REAGENT or RESOURCE	SOURCE	IDENTIFIER
Bis-(1,3-Diethylthiobarbituric Acid) Trimethine Oxonol ($DISBAC_2(3)$)	Thermo Fisher Scientific	Cat#: B413
Fluorescein-5-(and-6)-Sulfonic Acid, Trisodium Salt (FS)	Thermo Fisher Scientific	Cat#: F1130
RNeasy Plant Mini Kit	QIAGEN	Cat#: 74904
RNase-free DNase I set	QIAGEN	Cat#: 79254
Phusion Flash High-Fidelity PCR Master Mix	Thermo Fisher Scientific	Cat#: F548L
Deposited data		
Phosphoproteomics raw data	This paper	Proteomics data are deposited at Proteome Exchange (PRIDE): PXD038369 and PXD038363
Phosphoproteomics raw data (*tmk1-1*, *abp1TD*)	Friml et al.[19]	PRIDE: PXD031063
Transcriptomes sequencing reads	This paper	NCBI Sequence Read Archive (SRA): PRJNA881051
Phylogeny of B4 RAF-like kinases	This paper	Interactive Tree Of Life (iTOL): https://itol.embl.de/shared/dolfweijers
Experimental models: Organisms/strains		
Marchantia polymorpha; Tak-1 (wild-type)	Ishizaki et al.[106]	N/A
Marchantia polymorpha; $praf^{ko}$	Koide et al.[75]	N/A
Marchantia polymorpha; $praf^{ko}$ pPRAF::PRAF-mCitrine	This paper	N/A
Klebsormidium nitens (Kützing) Lokhorst; NIES-2285 (wild-type)	National Institute for Environmental Studies Microbial Culture Collection (JP)	Strain#: NIES-2285
Physcomitrium patens; Gransden (wild-type)	Ashton and Cove[107]	N/A
Penium margaritaceum; Skidmore isolate #8 of Skidmore College Culture Collection	Jiao et al.[65]	Maintained by David S. Domozych (Skidmore College, Saratoga Springs, NY 12866; ddomoz@skidmore.edu)
Arabidopsis thaliana; Col-0 (wild-type)	Widely distributed	N/A
Arabidopsis thaliana; *raf* (published as $OK^{130null}$)	Lin et al.[68]	N/A
Arabidopsis thaliana; *raf* pRAF20::RAF20-sYFP	This paper	N/A
Arabidopsis thaliana; *raf* pRAF24::RAF24-sYFP	This paper	N/A
Arabidopsis thaliana; *afb1-3*	Savaldi-Goldstein et al.[108]	N/A
Oligonucleotides		
See Table S1	This paper	N/A
Recombinant DNA		
Plasmid: pPLV17	De Rybel et al.[109]	N/A
Plasmid: pPLV17; pRAF20::RAF20	This paper	N/A
Plasmid: pPLV17; pRAF24::RAF24	This paper	N/A
Plasmid: pMpGWB347	Ishizaki et al.[110]	N/A
Plasmid: pENTR/D-TOPO	Thermo Fisher Scientific	Cat#: K2400-20
Plasmid: pMpGWBx00	Ishizaki et al.[110]	N/A

(*Continued on next page*)

Continued

REAGENT or RESOURCE	SOURCE	IDENTIFIER
Software and algorithms		
MaxQuant software package v2.4.7.0	Tyanova et al.[111]	RRID:SCR_014485 https://www.maxquant.org/
Perseus v1.6.14.0	Tyanova et al.[112]	RRID:SCR_015753 https://www.maxquant.org/
R	R foundation	RRID:SCR_001905 https://www.r-project.org/
Minardo-Model (R)	Kaur et al.[66]	https://bit.ly/MinardoModel
DAVID	Sherman et al.[113]	https://david.ncifcrf.gov/tools.jsp
REVIGO	Supek et al.[114]	http://revigo.irb.hr/
Cytoscape v3.10.1	Shannon et al.[115]	RRID:SCR_003032 http://cytoscape.org
AlphaFold2	Jumper et al.[116]	https://alphafold.ebi.ac.uk/download
Orthofinder v2.5.4	Emms and Kelly[117]	https://github.com/davidemms/OrthoFinder
MatLab (version: 2021b)	The MathWorks Inc.	RRID:SCR_001622 http://www.mathworks.com/products/matlab/
ACORBA v1.2 software	Serre et al.[118]	https://sourceforge.net/projects/acorba
ImageJ (Version 1.52)	Schindelin et al.[119]	RRID:SCR_003070 https://imagej.nih.gov/ij/
Measure Rosette Area Tool (ImageJ macro)	Remote-ImageJ project	http://dev.mri.cnrs.fr/projects/remote-imagej/files
FastQC v0.11.9	Babraham Institute (UK)	www.bioinformatics.babraham.ac.uk/projects/fastqc
HISAT2 v2.1.0	Kim et al.[120]	http://daehwankimlab.github.io/hisat2/
SAMTOOLS v1.9	Danecek et al.[121]	http://www.htslib.org/
FeatureCounts v2.0.0	Liao et al.[122]	https://subread.sourceforge.net/
DEseq2	Love et al.[123]	https://bioconductor.org/packages/release/bioc/html/DESeq2.html
Other		
AuxPhos	This paper	Source code: https://github.com/WeijersLab/AuxPhos Webtool: https://weijerslab.shinyapps.io/AuxPhos
MAFFT v7.505	Nakamura et al.[124]	https://mafft.cbrc.jp/alignment/software/
IQtree v1.6.12	Kalyaanamoorthy et al.[125]; Hoang et al.[126]	http://www.iqtree.org/
Cytoplasmic streaming analysis algorithm	This paper	https://github.com/jorissprakel/RAF_track_analysis

RESOURCE AVAILABILITY

Lead contact

Further information, inquiries and requests for reagents, resources and data should be directed and will be fulfilled by the lead contact, Dolf Weijers (dolf.weijers@wur.nl).

Materials availability

All reagents generated in this study are available from the lead contact without restriction.

Data and code availability

- Phosphoproteome data are available in the ProteomeXchange PRIDE database: PXD038369 and PXD038363. Transcriptome data are available in the NCBI Sequence Read Archive: PRJNA881051. Data underlying RAF-like kinase phylogeny is deposited

at the iTOL: https://itol.embl.de/shared/dolfweijers. This paper analyzes existing, publicly available data phospho-proteome data. The accession number for the datasets are listed in the key resources table.

- Code for the AuxPhos app and for MATlab code for analysis of cytoplasmic streaming are available at Github: https://github.com/WeijersLab/AuxPhos and https://github.com/jorissprakel/RAF_track_analysis.
- Any additional information required to reanalyze the data reported in this paper is available from the lead author upon request.

EXPERIMENTAL MODEL AND SUBJECT DETAILS

Plant material and culture conditions

All plants were cultured under 90-100 μmol photons m^{-2} s^{-1} white light with a 16 h light / 8 dark cycle at 22 °C and 75% humidity. *Arabidopsis thaliana* wild type Columbia-0 (Col-0) and all Arabidopsis mutants and transgenics were cultured on half strength Murashige and Skoog (MS) basal medium[127] at pH 5.7 supplemented with 0.8 % agar. The Arabidopsis *raf* was published as $OK^{130null}$ in Lin et al.[68]

Marchantia polymorpha wild type strain Takaragaike-1 (Tak-1) and all Marchantia mutants and transgenics were cultured on half strength Gamborg's B5 medium (B5 medium,[128]) pH 5.7 supplemented with 1% agar. The Marchantia *praf* mutant was previously published as $Mppraf^{ko}$.[75]

Klebsormidium nitens (NIES-2285) and *Physcomitrium patens* (Gransden strain) was cultured on BCD medium[129] supplemented with 1 % agar under the same condition as M. polymorpha. *Penium margaritaceum* was cultured in liquid Woods Hole medium[105] at pH 7.2 under gentle agitation (60RPM) at 20 °C with a 16 h light / 8 dark cycle, 30 – 50 μmol photons m^{-2} s^{-1} light in 50 ml Erlenmeyer flasks.

METHOD DETAILS

Generation of transgenics

Primers used in this study can be found in Table S1. Arabidopsis RAF reporter lines for RAF20 and RAF24 under their endogenous promoter were generated by amplifying the genomic fragment including the 3.5 kb region upstream of the start codon using the appropriate primers for each gene. Fragments were cloned into a pGIIK LIC-sYFP (pPLV17) vector[109] using the HiFi cloning kit (ThermoFisher).

For the Marchantia PRAF reporter line, a DNA fragment for an Arabidopsis-codon-optimized mCitrine coding sequence (CDS) was synthesized (IDT) and used to amplify a GGS2 linker-containing fragment by PCR with a primer set, pUGW2_Aor_GGS2_mCit_IF_F and pUGW2_Aor_mCit_IF_R, which was then cloned into the Aor51HI site in pUGW2 35S[110] using the In-Fusion cloning kit (TaKaRa Bio). The 2.5-kb HindIII-SacI fragment in the resulting plasmid, including the Gateway cassette followed by the GGS × 2 linker-attached mCitrine CDS, was ligated with the HindIII- and SacI-digested pMpGWBx00[110] to generate pMpGWBx47. The MpPRAF genomic sequence covering its promoter and CDS (without stop codon) in pENTR/D-TOPO_PRAF[75] was transferred to pMpGWB347 to generate pMpGWB347-PRAF. Agrobacterium GV2260 containing pMpGWB347-PRAF was used to transform $praf^{ko}$ plants[75] by the thallus transformation method.[130]

Imaging of transgenic lines plants for RAF-localization analysis

Marchantia gemmae expressing PRAF-mCitrine under endogenous promoter and 7 day-old Arabidopsis roots expressing RAF20-sYFP or RAF24-sYFP under their respective endogenous promoter were imaged using a Leica SP5 or SP8 confocal microscope equipped with an Argon laser (SP5) or a white light laser (SP8). Both, mCitrine and sYFP were excited at 514 nm, and emission was collected between 525-575 nm. Images were analyzed using ImageJ (Version 1.52).

Phosphoproteomics Sample preparation

Arabidopsis seedlings were vertically grown for 5 days as described above. For treatments, 100 nM IAA, 100 nM or 1 μM 1-NAA, 100 nM or 1 μM 2-NAA, 100 nM 2,4-D, 100 nM or 1 μM Benzoic Acid (BA), 100 nM Formic Acid (FA; all dissolved in DMSO) or an equal volume of DMSO was diluted in liquid half-strength MS medium. Plates were treated one at a time, placed horizontally, and solution was slowly added until roots were submerged. Plates were subsequently placed vertically again, to minimize gravitropic stimulation. Roots were harvested by scalpel and directly frozen in liquid nitrogen. Roots were ground to a fine powder and kept at -80 °C until further processing. For comparisons between chemicals, timepoints and genotypes, all replicates of all treatments were grown on the same day and processed independently.

For other species phosphoproteomics was carried out as described in above with the following adjustments: *Klebsormidium nitens*, *Physcomitrium patens* and *Marchantia polymorpha* were grown for 10 days on plates as described above, then treated with 100 nM IAA or DMSO in the respective growth medium for 2 minutes, harvested and frozen in liquid nitrogen. *Penium margaritaceum* was grown for 15 days as described above. Cells were collected by centrifugation at 1620 g for 2 min and washed 3 times with 10 ml of WHM to remove any residual extracellular polysaccharides from the cell surface. The pellet was resuspended in 10 ml of media and cells were treated with 100 nM IAA or DMSO for 2 min, harvested by centrifugation at 1620 g for 2 min and frozen in liquid nitrogen.

Sample preparation and data analysis was carried out as described above with the following adjustments: for *Marchantia polymorpha* the UP000244005 proteome was used, for *Physcomitrium patens* the UP000006727 proteome was used, for *Klebsormidium nitens* the UP000054558 proteome was used and for *Penium margaritaceum* the proteome from a whole genome assembly was used.[65]

Phosphopeptide enrichment

For phosphopeptide enrichment, ground Arabidopsis root powder was suspended in an extraction buffer with 100 mM Tris-HCl pH 8.0, 7 M Urea, 1% Triton-X, 10 mM DTT, 10 U/ml DNase I (Roche), 1 mM $MgCl_2$ and 1% benzonase (Novagen). The suspended lysate was sonicated using a cooled (4°C) waterbath sonicator (Qsonica) using 30 cycles of 30 seconds ON and 30 seconds OFF at 90% amplitude. Lysate was subsequently spun down using a cooled (4°C) tabletop centrifuge at 20.000xg for 30 minutes. After centrifugation, supernatant was collected and an extra 1% (v:v) of benzonase was added and incubated for 30 minutes at room temperature. Acrylamide was added to 50 mM and incubated for an extra 30 minutes at room temperature. After alkylation, proteins were precipitated using methanol/chloroform. To the lysate, 4 volumes of methanol, 1 volume of chloroform and 3 volumes of milliQ was added with rigorous vortexing in between. Lysate was centrifuged for 10 minutes at 5000 rpm. After centrifugation, the top layer was discarded and 3 volumes of methanol were added to further precipitate the protein layer by centrifugation for 10 minutes at 5000 rpm. After centrifugation, the supernatant was discarded and protein pellet was air dried. Proteins were next resuspended in 50 mM ammonium bicarbonate (ABC) and sonicated using a cooled (4°C) waterbath sonicator (Qsonica) using 30 cycles of 30 seconds ON and 30 seconds OFF at 90% amplitude. After sonication, protein concentration was measured by Bradford reagent (Biorad). For every biological replicate, 500 μg protein was digested with sequencing grade trypsin (1:100 trypsin:protein; Roche) overnight at room temperature. Next, peptides were desalted and concentrated using home-made C18 microcolumns. For peptide desalting and concentrating, disposable 1000 μl pipette tips were fitted with 4 plugs of C18 octadecyl 47 mm Disks 2215 (Empore™) material and 1 mg:10 μg of LiChroprep® RP-18 (Merck): peptides. Tips were sequentially washed with 100 % methanol, 80 % Acetonitrile (CAN) in 0.1% formic acid and twice equilibrated with 0.1 % formic acid. All chromatographic steps were performed by centrifugation for 4 minutes at 1500xg. After equilibration, peptides were loaded for 20 minutes at 400xg. Bound peptides were washed with 0.1% formic acid and eluted with 80 % ACN in 0.1 % formic acid for 4 minutes at 1500xg. Eluted peptides were suspended in loading buffer (80 % acetonitrile, 5 % tri-fluor acetic acid (TFA)). For phosphopeptide enrichment, MagReSyn® Ti-IMAC beads (Resyn bioscience) were used. For every reaction, a 1:4 peptide:bead ratio was used. Beads were equilibrated in loading buffer, resuspended peptides were added and incubated for 20 minutes at room temperature with slow mixing. After 20 minutes, bead-bound phosphopeptides were washed once in loading buffer, once in 80 % acetonitrile, 1 % TFA, and once in 10 % acetonitrile, 0.2 % TFA. After washing, phosphopeptides were eluted twice with 50 ul 1 % NH_4OH. After the last elution, phosphopeptides were acidified using 10 % formic acid. Phosphopeptides were subsequently concentrated using home-made C18 microcolumns. For peptide desalting and concentrating, disposable 200 μl pipette tips were fitted with 2 plugs of C18 octadecyl 47 mm Disks 2215 *(Empore™)* material and 1 mg:10 μg of LiChroprep® RP-18 (Merck): peptides. Tips were sequentially washed and equilibrated as described above. After equilibration, peptides were loaded for 20 minutes at 400xg. Bound peptides were washed with 0.1 % formic acid and eluted with 80 % ACN in 0.1 % formic acid for 4 min at 1500xg. Eluted peptides were subsequently concentrated using a vacuum concentrator for 30-60 minutes at 45°C and resuspended in 15μl of 0.1 % formic acid.

Filter-aided sample preparation and peptide fractionation

For FASP, 30kDa cut-off amicon filter units (Merck Millipore) were used. Filters were first washed by appling 50μl urea buffer UT buffer (8M Urea and 100mM Tris pH8.5) and centrifuging for 10 minutes on 11000 RPM at 20°C. The desired amount of protein sample (100μg) was next mixed with UT buffer until a volume of 200 μl, applied to the filter and centrifuged for 15 minutes on 11000 RPM at 20°C. Filter was washed with UT buffer by centrifugation for 15 minutes on 11000RPM at 20°C. Retained proteins were alkylated with 50mM acrylamide (Sigma) in UT buffer for 30 minutes at 20°C while gently shaking. Filter was centrifuged and after that washed trice with UT buffer for 15 minutes on 11000RPM at 20°C. Next filter was washed trice in 50mM ABC buffer. After the last wash, proteins were cleaved by adding sequencing grade trypsin (Roche) in a 1:100 trypsin:protein ratio. Digestion was completed overnight. The following day the filter was placed into a new tube and peptides were eluted by centrifuging for 15 minutes on 11000RPM at 20°C. Further elution was completed by adding two times 50mM ABC buffer and centrifuging for 10 minutes on 11000RPM at 20°C.

FASP digested peptides (10 μg) were submitted to offline in stage-tip high pH reversed phase (Hp-RP) fractionation. For Hp-RP tips, 2 plugs of C18 octadecyl 47mm Disks 2215 *(Empore™)* material and 1 mg:10 μg of LiChroprep® RP-18 (Merck): peptide were added to a 200 μl tip. Tips were washed with methanol for 4 minutes at 1000xg. Next buffer containing 0.1% formic acid and 80% acetonitrile was added and centrifuged for 4 minutes at 1000xg. Final equilibration was achieved with two washes of 0.1% formic acid and two washes of 20 mM ammonium formate (Optima®) pH10 for 4 minutes at 1000xg. Peptides were suspended in 20mM ammonium formate pH10 before loading onto Hp-RP tip. Sample was loaded by centrifugation for 20 minutes at 400xg. Peptides were subsequently eluted with ammonium formate buffers containing 5%, 8%, 11%, 18% and 40% ACN.

Mass spectrometry

For nano liquid chromatography–tandem mass spectrometry (nLC–MS/MS) analysis 5 ul of peptide samples were loaded directly onto a 0.10 * 250 mm ReproSil-Pur 120 C18-AQ 1.9 μm beads analytical column (prepared in-house) at a constant pressure of 825 bar (flow rate of circa 700 nL/min) with 1 ml/l HCOOH in water and eluted at a flow of 0.5 ul/min with a 50 min linear gradient

from 9% to 34% acetonitrile in water with 1 ml/l formic acid with a Thermo EASY nanoLC1000. An electrospray potential of 3.5 kV was applied directly to the eluent via a stainless steel needle fitted into the waste line of a micro cross that was connected between the nLC and the analytical column. Full scan positive mode FTMS spectra were measured between m/z 380 and 1400 on a Exploris 480 (Thermo electron, San Jose, CA, USA) in the Orbitrap at resolution (60000). MS and MSMS AGC targets were set to 300%, 100% respectively or maximum ion injection times of 50 ms (MS) and 30 ms (MSMS) were used. HCD fragmented (Isolation width 1.2 m/z, 28% normalized collision energy) MSMS scans of 2-5+ charged peaks in the MS scan were recorded in data dependent mode in a cycle time of 1.1 s (Resolution 15000, threshold 2e4, 15 s exclusion duration for the selected m/z +/- 10 ppm).

The MaxQuant quantitative proteomics software package was used to analyse LC–MS data with all MS/MS spectra. The following settings were used: peptide and protein FDR $\leq$ 0.01; the proteome of *A. thaliana* (UniProt ID UP000006548) was used as the protein database; maximum missed cleavage was set at 2; variable modifications Oxidation (M), Acetyl (protein N-term), Deamidation (NQ), pPhospho (STY); fixed modification AcrylAmide (C); match between runs and label-free quantification options were selected.

Phosphoproteomics data analysis

Maxquant output was analyzed using Perseus or R. For time series analysis, the Maxquant output PhosphoSTY tab was imported in Perseus.[112] Data was filtered for reverse, contaminants, only identified by site and localization probability of $\geq$0.75. Intensity values were $\log_2$ transformed and filtered to contain at least 75% valid values in each group. Values were subsequently normalized by median column subtraction. Remaining missing values were imputed from a normal distribution using standard settings in Perseus (width: 0.3, down shift: 1.8). An FDR permutation-based ANOVA test was performed to identify significantly changing phosphosite profiles (FDR $\leq$0.01). To adjust for treatment response, all $\log_2$-transformed profiles from mock treatments were merged with the auxin-responsive profiles. Mock values were subsequently subtracted from auxin-responsive profiles to obtain normalized auxin-responsive phosphosite profiles.

Temporal ordering/cluster identification of the phosphosite profiles were done using the Minardo-Model in R.66 Cluster number was determined in a way that most profiles followed the cluster centroid, resulting in 24 clusters.

Gene ontology enrichment was performed using the database for annotation, visualization and integrated discovery (DAVID).[113,131] For this, UniProt accession codes were used with duplicates removed. As a background, the full *Arabidopsis thaliana* proteome was used. Next REVIGO[114] and R were used to reduce overlapping GO-terms.

For kinase network analysis, $\log_2$-transformed phosphosite profiles of kinases with phosphosites in the activation loop (as described in Montes et al.[67]) were compared against all FDR significant (FDR$\leq$0.01) profiles using Pearson correlation and Euclidean distance (to also include time offset profiles). Profiles passing a Pearson correlation threshold of $\geq$0.6 and Euclidian distance threshold of $\leq$2.5 were extracted for further network analysis. For network analysis, UniProt accession codes were taken as an input for Cytoscape. Network analysis was performed in Cytoscape using standard settings. The degree and betweenness centrality were used to determine signaling hub importance.

Adobe illustrator and R, using standard packages, were used for visualization.

R shiny app

All the phosphosites and the corresponding enrichment data have been imported into the R environment as CSV files. DataTables, reshape2 and dplyr packages were used for data visualization and data wrangling. 3D protein structures of *Arabidopsis thaliana* proteome predicted through the AlphaFold2 program were downloaded from the AlphaFold database hosted at EBI (https://alphafold.ebi.ac.uk/download). These structures were rendered and visualized using the r3dmol package while the plots were generated using ggplot2 package in R.

Orthogroup construction

Identification of orthogroups i.e., common orthologous sequences between multiple species were estimated using Orthofinder.[117] Proteomes used for this analysis include: *Arabidopsis thaliana* (Araport11), *Marchantia polymorpha* (v6.1), *Physcomitrium patens* (v3.3), *Klebsormidium nitens* (v1.1) and *Penium margaritaceum* (v1).

Phylogenetic analysis of RAF family

A total of 104 proteomes from publicly available genomes were searched for homologs with HMM made from the alignment of *Arabidopsis thaliana* and *Marchantia polymorpha* RAF homologs as queries for the HMM profile. Obtained homologous sequences were aligned using MAFFT E-INS-i algorithm (v7.505).[124] Positions with more than 60% gaps were trimmed from the alignment using trimAl.[132] Phylogenetic tree was constructed using IQtree2 (v1.6.12)[126] with JTT+R10 as the model of evolution selected with ModelFinder[125] with a maximum of 1000 rapid bootstraps. Phylogenetic trees were visualized in iTOL (v5).[133]

Cytoplasmic streaming

Cytoplasmic streaming was recorded using a Leica SP5 or SP8 confocal microscope equipped with HyD detectors using Apo λ 63×/1.10 water immersion objective plus 6x digital zoom in an 256x256 pixel format. Cytoplasmic streaming was recorded and analyzed for Arabidopsis epidermal cells of the root elongation zone and Marchantia rhizoid cells using the following method: Seven day old Arabidopsis plate-grown seedlings were taken into the microscopy room and mitochondria were stained by transferring the seedling

into a petri dish with liquid ½ MS medium containing 1 μM Rhodamine 123 for 5 minutes. Subsequently, seedlings were washed with liquid ½ MS without Rhodamine 123. Seedlings were then transferred to microcopy slides in a drop of liquid ½ MS containing 100 nM or 1 μM, BA, IAA, 1-NAA or 2-NAA or the equivalent amount of solvent (DMSO), covered by a coverslip and left on the microscope stage to adapt to the environment for 30 minutes. Cytoplasmic streaming was recorded in at least 5 epidermal cells of the root elongation zone per root at a frame rate of 5.3 frames per second for 30 seconds (159 frames).

Prior to the experiment, Marchantia thallus was grown from gemmae for two days in liquid B5 medium in a petridish. After two days of cultivation Rhodamine 123 was added to a final concentration of 1 μM and Triton-X-100 was added to a final concentration of 0.01%. Marchantia samples were stained for 30 minutes and then washed three times with liquid B5 medium containing 0.01% Triton-X-100 without Rhodamine 123. Samples were then transferred to microscopy slides and cytoplasmic streaming in rhizoid cells was recorded as described for Arabidopsis.

Data analysis for cytoplasmic streaming

Data analysis was performed in MatLab (version: 2021b). First, static background signal was removed from the raw fluorescence images using a moving window median filter (averaging window = 25 frames) and motile objects smoothed with a 2-pixel Gaussian blur filter. Moving objects were tracked using an established particle tracking algorithm,[134] keeping only those trajectories whose length exceeds 3 seconds. For each cell, from the individual trajectories of the remaining moving objects, typically between 30 to 60 per time series, an ensemble-averaged mean-squared displacement was computed:

$$\Delta r^2(\tau) = \langle |r(t+\tau) - r(t)|^2 \rangle$$

Per cell, these mean-squared displacements were fitted to the anomalous diffusion model (ADM),[61,62] a generalization of Einstein's diffusion model to describe complex non-Fickian motion of organelles in the visco-elastic liquid of the cellular cytosol, which is composed of an unknown mixture of passive (Brownian) and active (streaming) transport in a crowded and heterogeneous medium:

$$\Delta r^2(\tau) = K\tau^{\alpha}$$

where τ is the correlation time. In the ADM, the generalized diffusion power law exponent α provides information on the average nature of the transport processes: $\alpha < 1$ is indicative of sub-diffusive motion, characteristic of Brownian motion in a visco-elastic liquid, $\alpha = 1$ indicates pure Brownian motion in a viscous liquid and > 1 , known as super-diffusion, indicates transport with an active, e.g., motor-protein driven, component. Intermediate values of the power law exponent α provide insight into the relative balance of these different processes on the organellar motion. The transport rate constant K (in units mm/s^a) informs about the average transport rate: the larger the value of K the faster the organellar transport in the cells. Our analysis yields one average value for α and K per cell; the significance of the differences between control and treatment was assessed with a two-sided Wilcoxon signed rank test.

Membrane potential measurement using $DISBAC_2(3)$

Membrane potential was measured using the $DISBAC_2(3)$ probe as previously described for Arabidopsis.[18] DISBAC2(3) (2 μM) was added to buffered ½ MS liquid medium with 1% (w/v) sucrose containing either 0 or 100 nM IAA. Five-day-old Arabidopsis seedlings were transferred to a sealable single-layer PDMS silicone chip.[18] The PDMS silicone chip containing the seedlings was then placed on a vertical spinning disk microscope for a 20-min recovery. During the recovery process, the seedlings were treated with control medium at a flow rate of 3 μl/min. Seedlings were imaged every 30 seconds with a x20/0.8 objective. DISBAC2(3) was excited with a 515-nm laser, and the emission was filtered with a 535/30-nm bandpass filter. DISBAC2(3) fluorescence was measured at the border between epidermis and cortical cells of the transition zone by selecting 5-6 or 3-4 cells for Col-0 and *raf*, respectively.

Membrane potential of Marchantia and Klebsormidium was measured using the same probe with the following modifications to the protocol: Marchantia gemmae were removed from gemmae cups and placed liquid B5 with 0.01%Triton-X-100 supplemented with 15 μM $DISBAC_2(3)$, vacuum infiltrated for 5 minutes and transferred to a cover slip followed by incubation for 30 minutes before imaging. Imaging was performed on an inverted Leica SP8 confocal microscope using the same setting as for Arabidopsis. Klebsormidium was grown for 10 days as described above. A small amount of Klebsormidium was then scraped off the plate and dissolved in liquid BCD medium supplemented with 15 μM $DISBAC_2(3)$ followed by incubation for 30 minutes before imaging.

Root surface pH profile

Root surface pH was measured using the ratiometric Fluorescein-5-(and-6)-Sulfonic Acid, Trisodium Salt (FS) (Invitrogen™ F1130).[81] Five-day-old Arabidopsis seedlings were transferred to unbuffered ½ MS medium containing 50 μM FS dye and either 0 or 100 nM IAA. Seedlings were allowed to recover on a vertical spinning disk microscope for 20 minutes after transfer to the microscope chamber. Imaging was performed using a vertical stage Zeiss Axio Observer 7 microscope coupled to a Yokogawa CSU-W1-T2 spinning disk unit with 50 μm pinholes, equipped with a VS-HOM1000 excitation light homogenizer (Visitron Systems). Images were acquired using VisiView software (Visitron Systems, v.4.4.0.14). We used a Zeiss Plan-Apochromat ×10/0.45 objective. FS was excited by 405 and 488 nm laser. The 488/405 nm fluorescence emission ratio along the root was calculated using the ATR software.[81]

Gravitropic response

The Arabidopsis root gravitropic experiment was performed as described[18]: 5-day-old seedlings were placed on the top of a thin layer of growth medium (½ MS, 1% (w/v) sucrose, 1% plant agar, Duchefa) in a 3D-printed microscopy chambered coverslip. The chamber was placed vertically on the vertical stage microscope for 45 minutes to recover, after which the chamber was rotated 90 degrees. Roots were imaged every minute for 1 hour. The angles of the root tips were measured using ACORBA v1.2 software.[118]

Phenotyping

Arabidopsis plant height was determined from 16 individual wild type and *raf*, RAF20 and RAF24 complementation lines senescing plants, seven weeks after germination.

Rosette area was determined from individual wild type and *raf* plants, and RAF20 and RAF24 complementation lines 28 days after germination. Plants were photographed individually using a Canon EOS 250D camera with EFS 18-135mm Macro Lens. Rosette area was then measured in ImageJ (Version 1.52) using the "Measure Rosette Area Tool" macro (http://dev.mri.cnrs.fr/projects/remote-imagej/files). To compare the ***germination efficiency*** between *raf* mutants and wild type, seeds for each genotype were surface sterilized, stratified in a 0.1% agarose solution for two days at 4°C and paced on half strength MS plates (0.8% Agar). Plates were grown vertically for 9 days and germinated seeds were scored at day 1, 2, 3, 4, 7 and 9. Germination percentages were calculated for each day. Germination efficiency was also determined for and RAF20 and RAF24 complementation lines. Herefore, seeds of and RAF20 and RAF24 complementation lines, *raf* mutants and wild type were prepared as described above and grown horizontally. The germination percentage was calculated after 3 days. The experiments were repeated at least three times individually and data were combined for analysis.

Germination

Seedlings of Arabidopsis wild type, *raf* , RAF20 and RAF24 complementation lines were germinated on half strength MS and vertically grown for 7 days. After seven days, 16 seedlings with representative root length for each genotype were transferred to new square petri dishes either containing 10 nM IAA, 100 nM IAA, 1000nM IAA or a mock treatment representing an equal amount of solvent (DMSO). ***Root length*** was captured by photographing the plates immediately after transferring the seedlings, after 24 hour, after 48 hours and after 120 hours, using a Canon EOS 250D camera with EFS 18-135mm Macro Lens. Root length was then measured in ImageJ using the segmented line tool and growth rates calculated.

Marchantia phenotyping

To compare the ***thallus growth*** between Marchantia *praf* mutants (n=44) and wild type (n=50), thalli were grown from gemmae on half strength Gamborg B5 medium. Plates were grown for 29 days and projected thallus area was captured by photographing the plates immediately after transferring the gemmae, after 2, 4, 7, 9, 11, 14, 16, 18, 22 and 29 days, using a Canon EOS 250D camera with EFS 18-135mm Macro Lens. Thallus area was then measured in ImageJ (Version 1.52) using the Polygon selection tool. For ***auxin sensitivity*** assays, Marchantia *praf* mutant (n=10) or wild-type (n=10) gemmae were grown on half strength Gamborg B5 medium supplemented the indicated concentration of IAA and grown for 10 days. At day 10, thallus size was captured by photographing the plates using a Canon EOS 250D with EFS 18-135mm Macro Lens. Thallus area was then measured in ImageJ (Version 1.52) using the Polygon selection tool. ***Gemma cup number*** was determined on *praf* mutants (n=20), wild type (n=20) and PRAF complementation (n=20) thalli after 24 days of growth on half-strength Gamborg B5 medium.

Transcriptomic analysis

Arabidopsis thaliana wild-type (Col-0) and mutant (*raf*) seeds were sown on half-strength MS medium covered with nylon mesh and vertically grown for 7 days. Plants were then submerged in liquid half-strength MS medium containing either 1 μM IAA or the equivalent amount of solvent (DMSO). Plates were kept horizontally for about 30 seconds and then kept vertically for 1 hour to incubate. After incubation, root tips were harvested using a scalpel and immediately frozen in liquid nitrogen.

Marchantia polymorpha wild-type (Tak-1) and mutant (*praf*) gemmae were placed on B5 solid medium covered with nylon mesh (100 mm pore) and grown for 9 days. After growing, plants were submerged in liquid B5 medium and cultured for 1 day. After pre-cultivation, IAA was added to a final concentration of 1 μM or an equivalent amount of DMSO was added and plants were incubated for 1 hour. Using a scalpel, thalli were harvested from the mesh, blotted on paper towels and immediately frozen in liquid nitrogen.

After harvesting, all frozen samples were ground into fine powder using a pre-cooled mortar and pestle. Total RNA form all samples was extracted using a RNeasy Plant Mini Kit (QIAGEN). Total RNA was treated with RNase-free DNase I set (QIAGEN). RNA-seq library construction and RNA sequencing were performed by BGI Tech Solutions (Hong Kong).

RNAseq data analysis

Up to 20 million paired-end 150 bp reads were collected for each sample. Quality assessment for raw reads was performed using FastQC (www.bioinformatics.babraham.ac.uk/projects/fastqc). For both *Arabidopsis thaliana* (Araport11[135]) and *Marchantia polymorpha* (v6.1[136]), reads were mapped onto the respective genomes using HISAT2 (v2.1.0;[120]) with additional parameters "–trim5 10 –dta". Alignment (SAM/BAM) files were sorted and indexed using SAMTOOLS (v1.9[137]). FeatureCounts (v2.0.0[122]) was used to count the reads mapped on to each gene, with the parameters "-t 'exon' -g 'gene_id' -Q 30 –primary -p -B -C" for Arabidopsis transcipts and "t 'gene' -g 'ID' -Q 30 –primary -p -B -C" for Marchantia transcripts. DEseq2[123] was used to normalize the raw counts and

perform the differential expression analysis with a design matrix including the interaction term (Padj<0.05). Data processing and statistical analysis was performed using R (https://www.r-project.org/). Sequenced raw reads were deposited in NCBI Sequence Read Archive (SRA) under the project accession number PRJNA881051.

QUANTIFICATION AND STATISTICAL ANALYSIS

Sample numbers and statistical analysis are detailed in each methods section above, and indicated in each figure legend.

CellPress
OPEN ACCESS

Supplemental figures

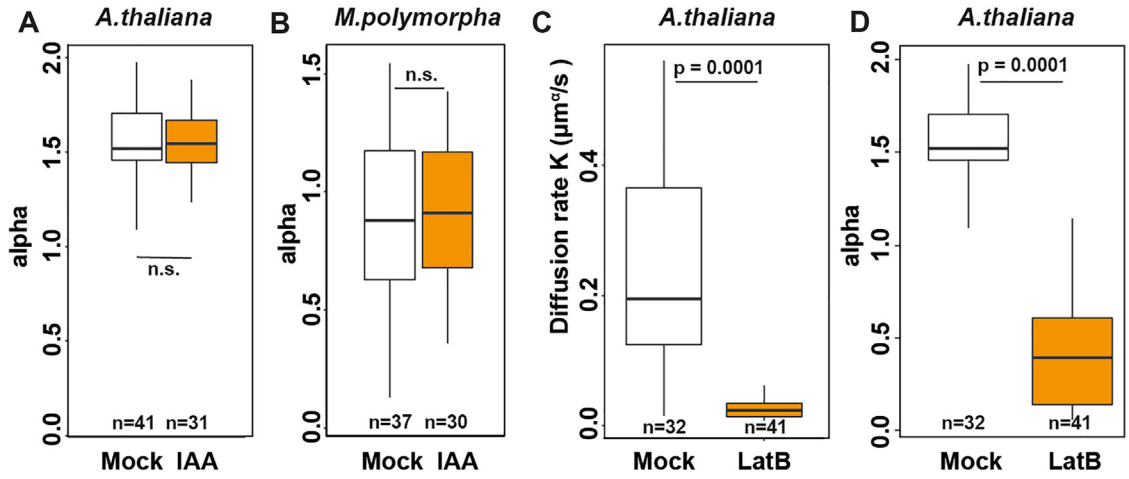

Figure S1. Characterization of cytoplasmic streaming, related to Figure 1

(A and B) (A) Quantification of the diffusive component (α) of cytoplasmic streaming in wild-type Arabidopsis roots and (B) Marchantia rhizoid cells with and without auxin treatment.

(C and D) Diffusion rate (K; C) and diffusive exponent (α; D) of cytoplasmic streaming in wild-type Arabidopsis roots treated with mock medium or latrunculin B. Boxplots are shown along individual measurements, number of observations (n) is indicated, and significance (Student's t test) is shown.

A

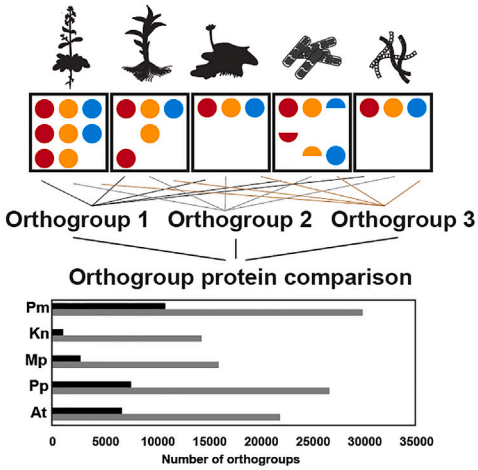

B

Orthogroup	ATG code	Description
OG0000102	AT1G08720	Serine/threonine-protein kinase EDR1
OG0000257	AT1G06070	bZIP transcription factor
OG0000323	AT1G07350	Serine/arginine-rich splicing factor SR45a
OG0000502	AT2G16640	Translocase of chloroplast 132
OG0000557	AT1G23860	Serine/arginine-rich splicing factor RSZ21
OG0000647	AT3G45780	Phototropin-1
OG0001209	AT3G60240	Eukaryotic translation initiation factor 4G
OG0001903	AT1G13020	Eukaryotic translation initiation factor 4B2
OG0002206	AT1G21160	Eukaryotic translation initiation factor 5B
OG0002707	AT3G48860	Coiled-coil domain-containing protein SCD2
OG0003358	AT1G13950	Eukaryotic translation initiation factor 5A-1

C

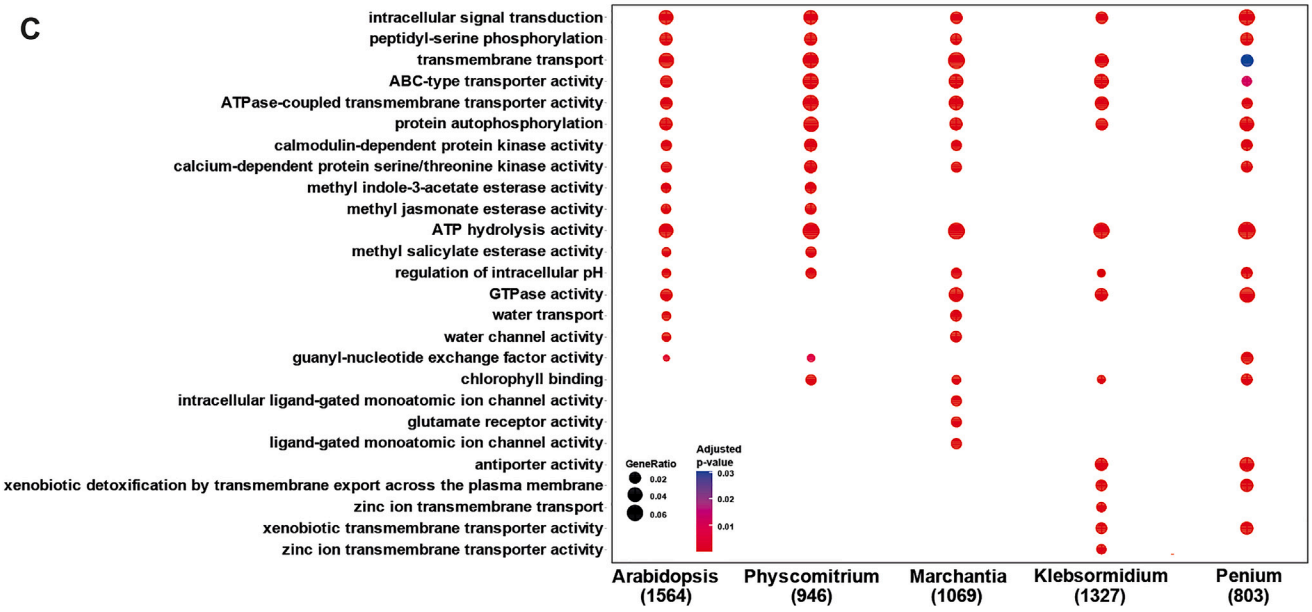

Figure S2. Comparative analysis of auxin-triggered changes in phosphoproteomes across species, related to Figure 2

(A) Strategy for orthogroup construction based on protein sequence across the 5 species used here (top). The lower panel shows the number proteins in shared (black) and unique (gray) orthogroups in each species.

(B) List of the 11 orthogroups shared between all species, alongside ATG code of an Arabidopsis member in each orthogroup and its functional description.

(C) GO-term analysis of FDR significant orthogroups of all species tested identified in phosphoproteomics.

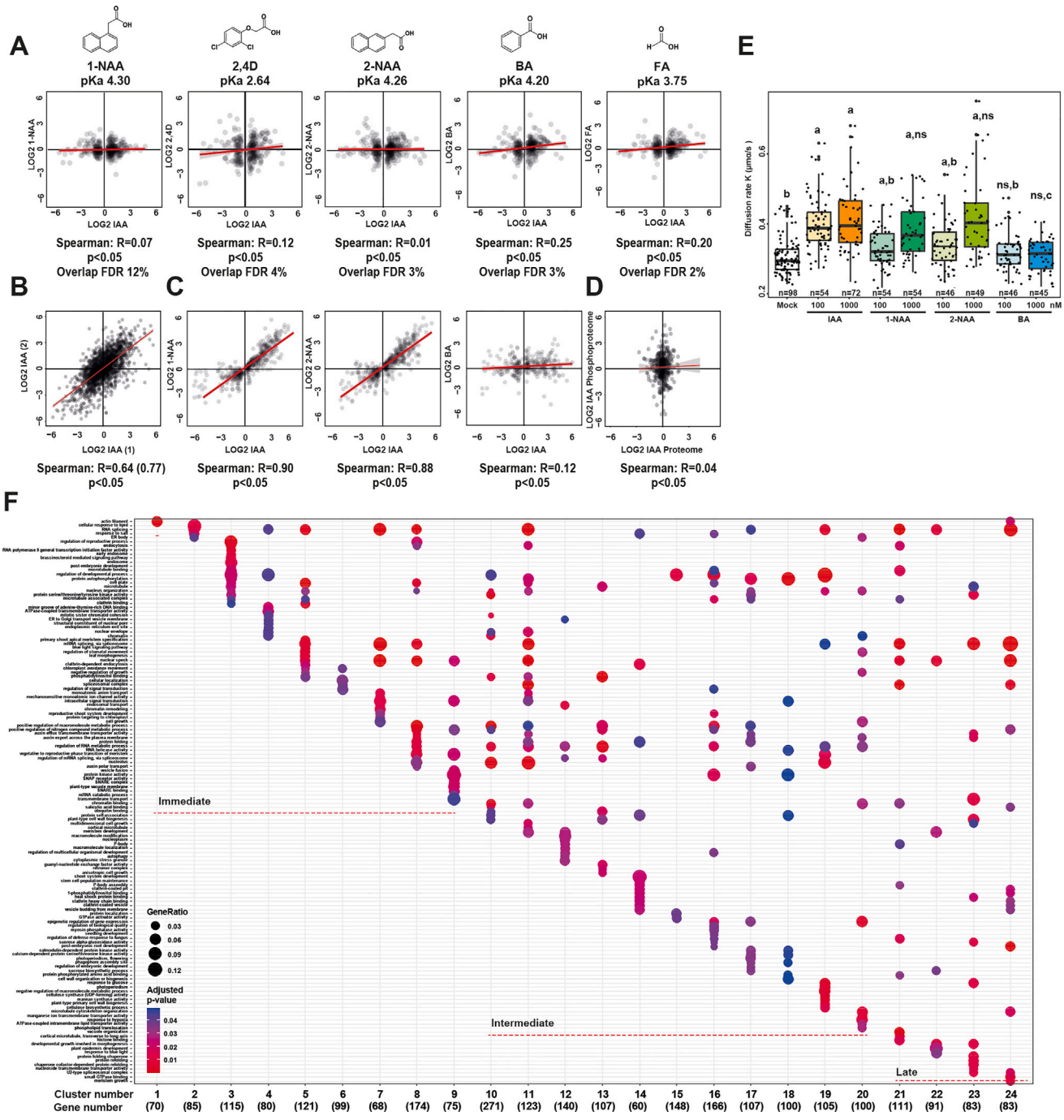

Figure S3. Specificity and dynamics of auxin-triggered phospho-response, related to Figure 3

(A) Plots comparing differential phosphosites (FDR $\leq$ 0.05) in 2 min 100 nM IAA treatment (x axes) with fold-change of corresponding phosphosites in similar treatments with other compounds. Structures and pKa values are given for each compound. Red line indicates regression line (with confidence interval in gray), and Spearman correlation value is indicated underneath each plot.

(B) Correlation plot of two independent IAA phosphoproteome experiments. Spearman correlation of all sites is 0.64 while it is 0.77 when considering only differential sites at FDR $\leq$ 0.05.

(C) Plots comparing differential phosphosites (FDR $\leq$ 0.05) in 2 min 100 nM IAA treatment (x axes) with fold-change of corresponding phosphosites in 2 min treatment of 1 µM of other compounds. Structures and pKa values are given for each compound. Red line indicates regression line (with confidence interval in gray), and Spearman correlation value is indicated in each plot.

(legend continued on next page)

(D) Correlation between fold-changes in IAA-trigged shotgun proteome (x axis) and phosphoproteome (y axis) both treated with 100 nM IAA for 2 min. Red line is regression line with confidence interval (gray).
(E) Cytoplasmic streaming in Arabidopsis wild-type (Col-0) root epidermis cells treated with mock, IAA, 1-NAA, 2-NAA, or BA at a concentration of either 100 nM or 1 μM. Displayed is diffusion rate K ($\mu m^2/s$). Boxplots are shown along individual measurements, and significance (Student's t test) is shown.
(F) GO-term analysis of each cluster identified in Figure 3C.

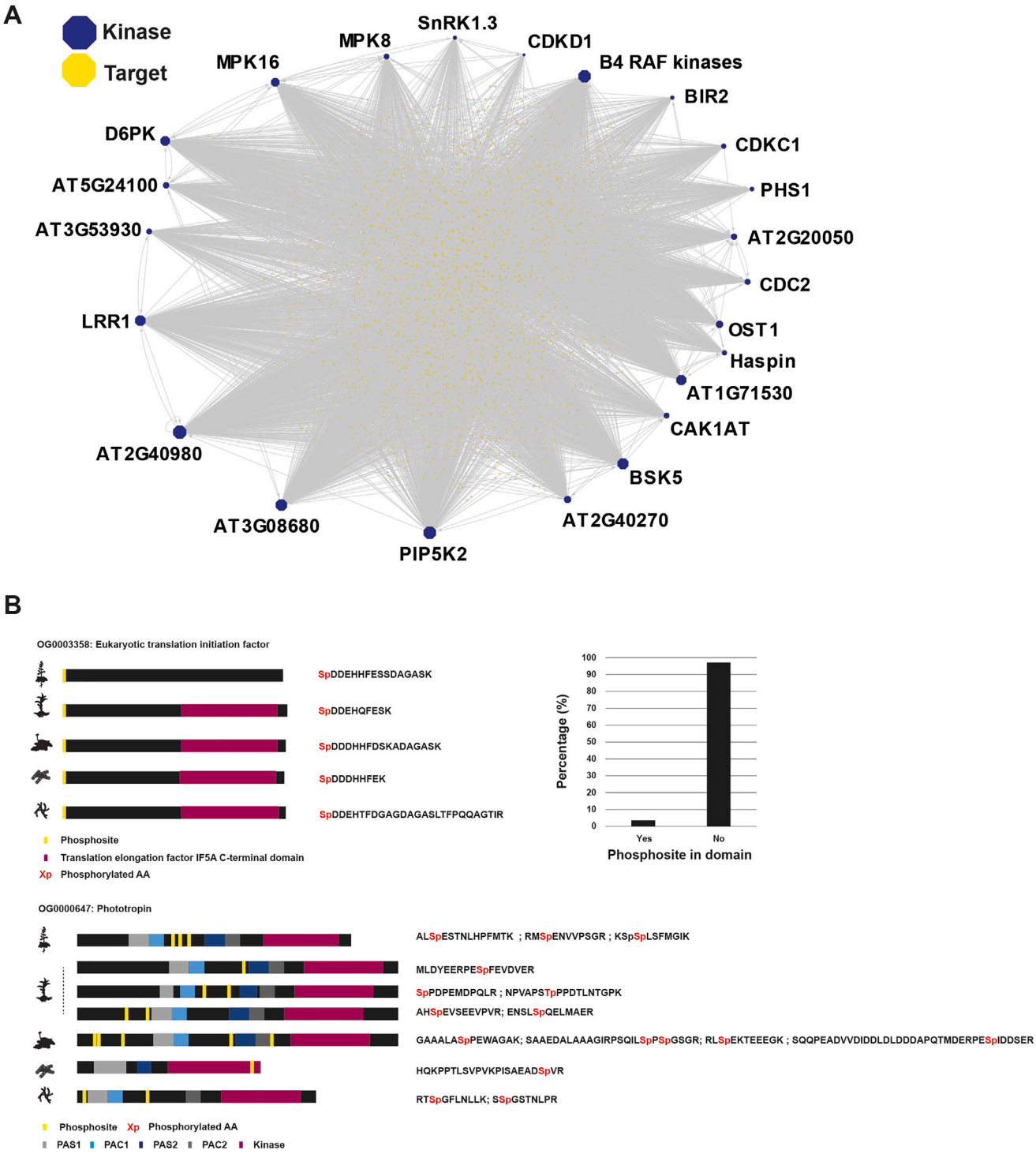

Figure S4. Inferred kinase-substrate network, related to Figure 4

(A) Kinase network of the 23 identified kinases with phosphoregulation in their activation loop. Kinases are depicted in blue, whereas substrates are depicted in yellow. Sizes of hexagons are based on degree.

(B) Comparison of the location and sequence of phosphosites among phospho-targets conserved in all species tested. Displayed are the domain structures of the proteins and the position of the phosphosites within the protein of two examples (left). The posphopeptide sequence is shown, and the phosphorylated amino acid is highlighted (middle). Quantification of the fraction of phosphosites located in a domain or not is given for all phosphosites in conserved phospho-targets (right). A full list comparing all phosphosites in the conserved phospho-target can be found in Data S1.

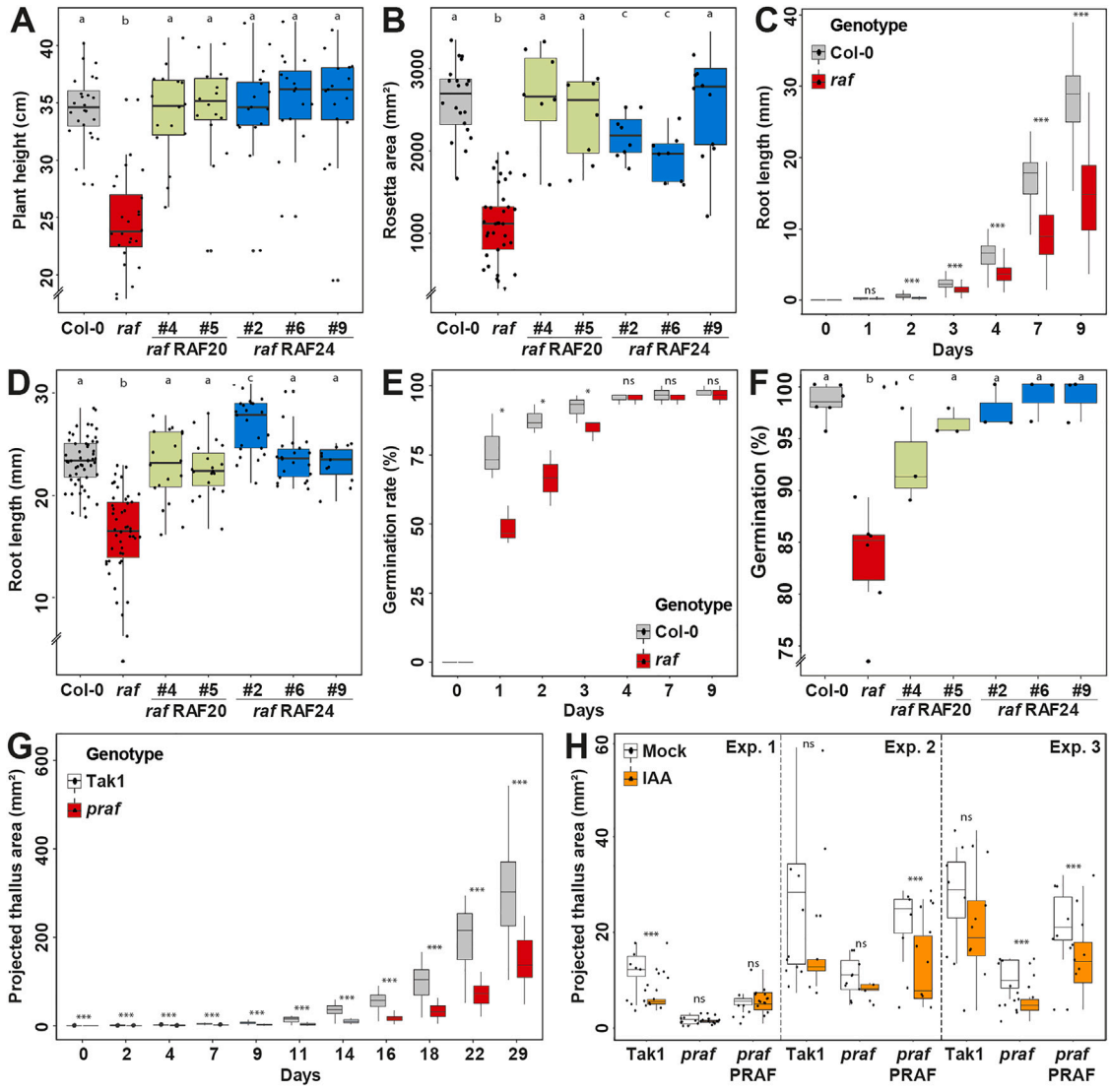

Figure S5. Phenotypic analysis of *raf* mutants in Arabidopsis and Marchantia, related to Figure 5

(A–F) Characterization of phenotypes related to growth and development in Arabidopsis wild type (Col-0), *raf* mutant, and complemented *raf* mutant (with RAF20 of RAF24 transgene; multiple independent lines each) and (G) in Marchantia wild type (Tak1) and *praf* mutant. (A) Flowering plant height, (B) rosette area, (C) root length followed over 9 days in wild type and mutant and at 7 days in all genotypes (D). (E) Germination rate over 9 days in wild type and mutant and after 3 days in all genotypes (F).

(G) Projected thallus area in wild-type and mutant Marchantia thallus, followed over 29 days.

(H) Quantification of IAA-induced thallus growth inhibition in wild-type Marchantia (Tak1), *praf* mutant, and *praf* mutant complemented with PRAF transgene, across three independent experiments. (A, B, D, F, and H) Boxplots are shown along individual measurements and (A, B, D, and F) significance (Student's t test) is shown, "a" indicates no significant difference to mutant, "b" indicates significant difference to wild type, and "c" indicates significant difference to both wild type and mutant ($p < 0.001$, ns, not significant). (C, E, and G) Boxplots are shown along individual measurements, and significance (Student's t test) is shown (*** $p < 0.001$). (H) Significance (Student's t test) is shown to corresponding 0 nM IAA treatment (*** $p < 0.001$, ** $p < 0.01$, * $p < 0.05$, ns, not significant).

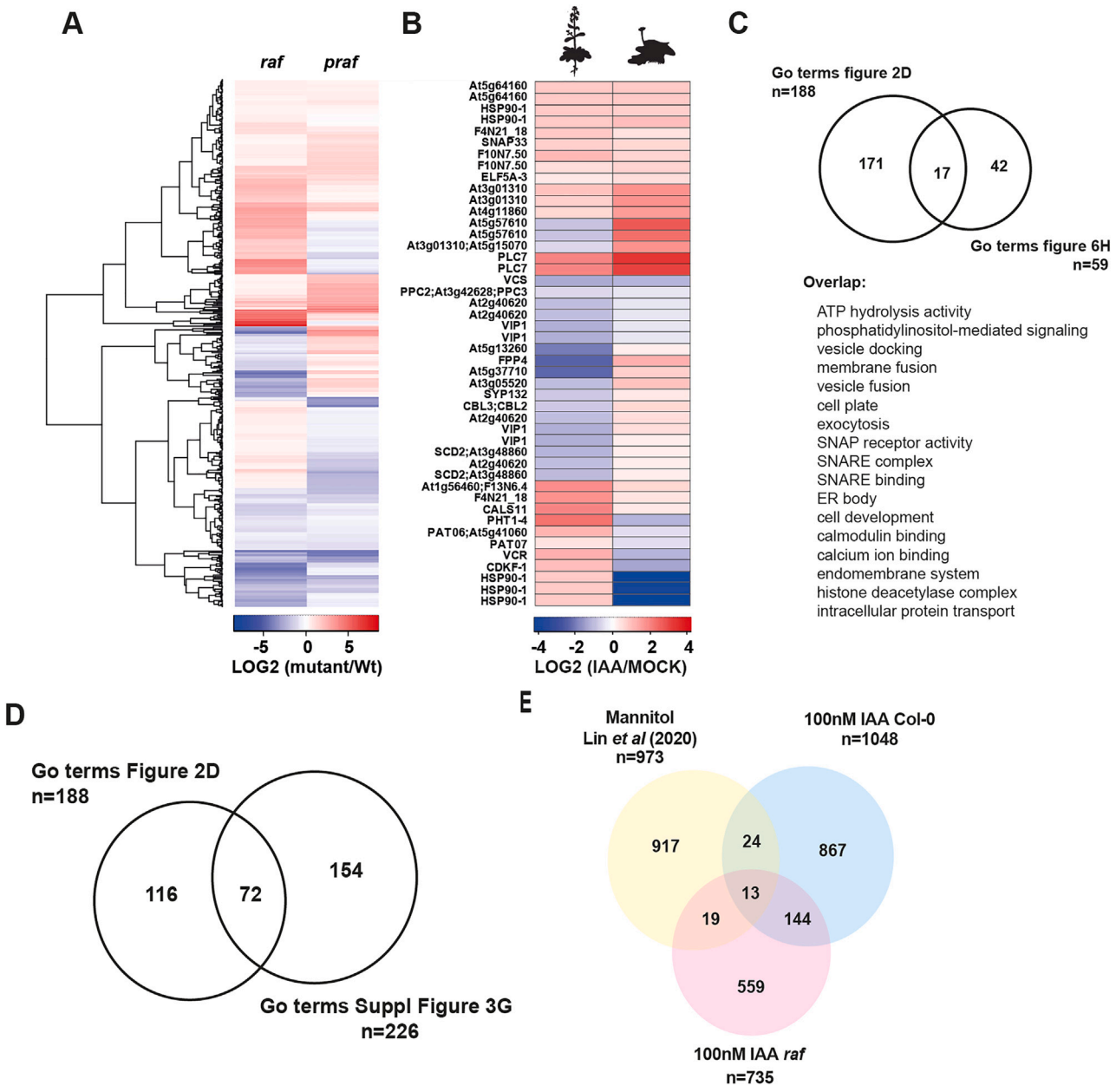

Figure S6. Analysis of *raf* mutant phosphoproteomes, related to Figure 6

(A) Overlap of potential RAF targets in Arabidopsis and Marchantia, based on differential phosphorylation in *raf* and *praf* phosphoproteomes under mock conditions, compared with wild types.

(B) Differential phosphorylation patterns upon IAA treatment in wild-type Arabidopsis and Marchantia (2 min) of orthologous proteins commonly dependent on RAF in both species. Note that some orthogroups contain more than one member in Arabidopsis.

(C) Venn diagram showing the overlap between GO-terms enriched for land plants, bryophytes, and algae (Figure 2D) and GO-terms enriched for overlapping and conserved auxin- and (P)RAF-dependent phosphorylated proteins (Figure 6H). The list shows the overlapping GO terms.

(D) Venn diagram displaying the overlap between GO-terms enriched for land plants, bryophytes, and algae (Figure 2D) and GO-terms enriched for all clusters of the time series (Figures 3C and S3G). The description of overlapping GO terms can be found in Data S1.

(E) Venn diagram showing overlap between phosphosites differentially regulated (≤ 0.05) in mannitol-treated Arabidopsis plants,[68] 100 nM IAA treated Col-0 and 100 nM treated *raf* mutant.

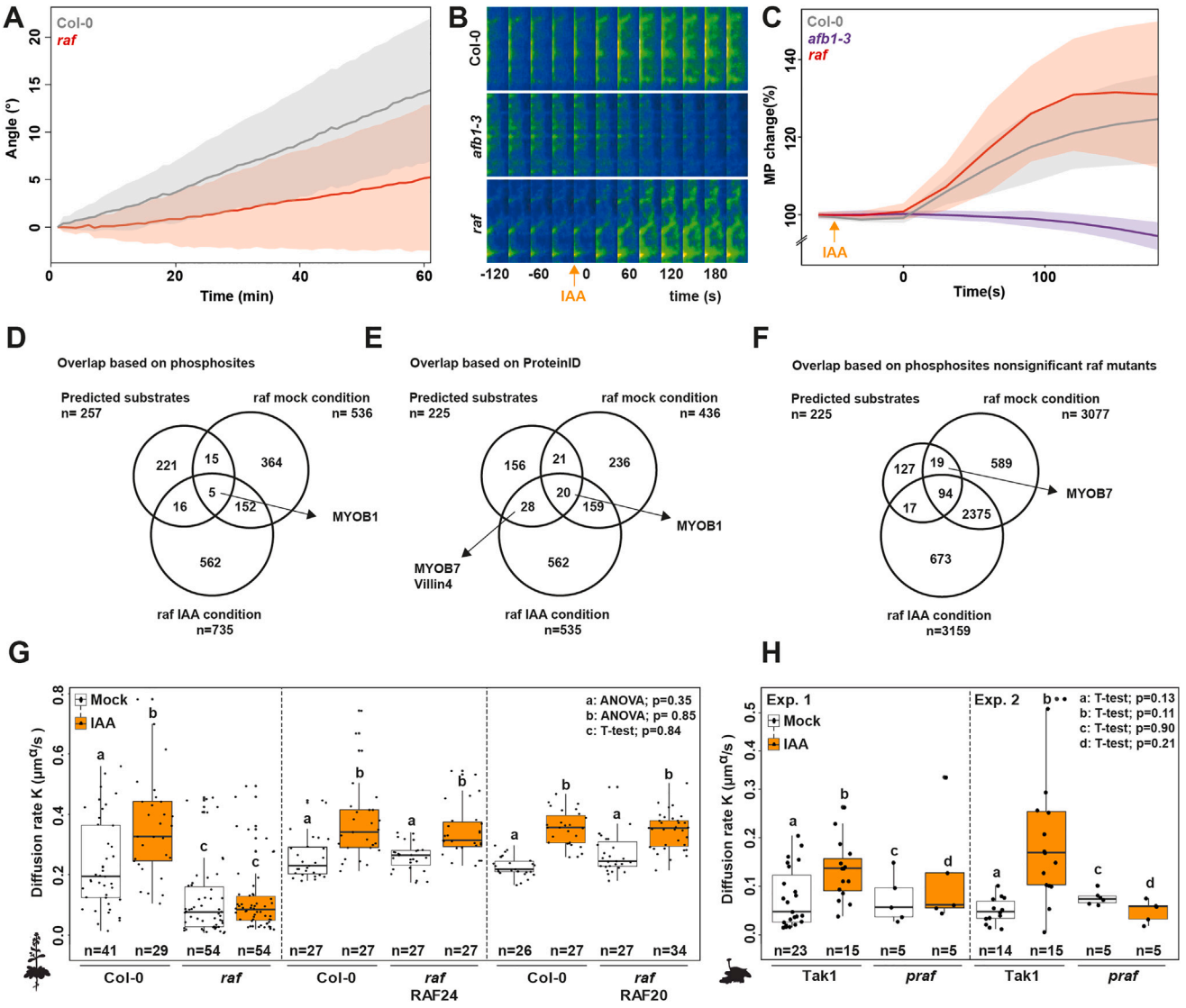

Figure S7. RAF-like kinases link rapid phospho-response to fast auxin responses, related to Figure 7

(A) Angle of root tip bending of Arabidopsis wild type (Col-0) and *raf* mutant seedlings after gravitropic stimulation over time. Solid lines show average, and shaded areas confidence intervals across 26–28 roots for each genotype.

(B and C) (B) Representative images and (C) quantification of changes in of DISBAC2(3) fluorescence intensity in the elongation zone of roots from wild type (Col-0), *afb1-3*, and *raf* mutant before and after IAA treatment. Solid lines show average, and shaded areas confidence intervals across 10 roots for each genotype. (D–F) Venn diagrams showing overlap between predicted RAF-substate phosphosites (D) or phosphoproteins (E and F) and (D) phosphosites or (E) phosphoproteins differentially regulated (≤ 0.05), and (F) all proteins detected but not significantly enriched in *raf* mutants under mock of IAA conditions.

(G and H) Cytoplasmic streaming in mock and mock- or IAA-treated root epidermal cells in Arabidopsis wild type (Col-0), *raf* mutants, and *raf* mutant complemented with RAF20 or RAF24 transgenes (G) and Marchantia wild-type (Tak1, H) and *praf* mutant rhizoid cells. Displayed is the diffusion rate K ($\mu m^{\alpha}/s$). Boxplots are shown along individual measurements, number of observations (n) is indicated, and significance (Student's t test or ANOVA) is shown. Dashed lines indicated independent experiments (note that for E, a selection of the data has been compiled and shown in Figures 1 and 7).